Mechanical and microstructural developments and relations in upset butt welding of highly formable steel grade HR45

B.J.A. Jol

Master's thesis

NIMR project MC.8.03174

Supervisors:
Ir. N.F.H. Kerstens
Prof. Dr. I.M. Richardson

Delft University of Technology

Netherlands Institute for Metal Research

Fontijne Grotnes B.V.

Delft University of Technology

Netherlands Institute
for Metals Research

Table of contents

Samenvatting

Bij het maken van velgen wordt er gestreefd naar een lager gewicht van de velg. Hiervoor wordt een nieuwe staalsoort onderzocht, dat als kwaliteiten een hoge sterkte en vervormbaarheid heeft: HR45. Tijdens het vormen van het profiel in de las treedt er echter regelmatig scheurgroei vanuit de laszone op. De vraag is of dit mechanisch gedrag voortkomt uit een lasproces dat de delen niet goed verbindt of een microstructuur die niet zo vervormbaar is als de las en dus eerder mechanisch falen vertoont.

Het proces werkt met een elektrische stroomdoorvoer door een relatief groot lasoppervlak, die het materiaal verwarmt tot een bepaalde temperatuur waarbij het makkelijk te vervormen wordt. Wanneer deze temperatuur bereikt is worden de oppervlakken aan elkaar gesmeed met een kracht die loodrecht op het lasoppervlak staat. In principe treedt hierbij geen smelten op en is dus een vaste stof proces.

In dit onderzoek zijn lassen gelegd bij verschillende lasinstellingen (de kracht en stroom waarbij gelast wordt), zodat bestudeerd kon worden wat momenteel de uitdagingen zijn in dit proces. De belangrijkste factoren hierbij bleken de uitlijning van de te lassen platen, de lastemperatuur en regelmatige maar niet gelijke verdeling van de warmteinvoer.

De uitlijning is voornamelijk belangrijk voor de goede vorm van de las, maar ook voor de materiaalstromingen tijdens het smeedproces, waarbij de oppervlaktevervuilingen verdeeld dienen te worden over de laszone.

Deze stromingen zijn tevens afhankelijk van de lastemperatuur, die zodanig moet zijn dat het materiaal verzacht is. Bij lagere temperaturen is het materiaal wel smeedbaar, maar de stromingen zijn dusdanig dat de vervuilingen initiatiepunten zijn voor scheurvorming. Een temperatuur waarbij het materiaal verzacht is en niet alleen smeedbaar is, is dus gewenst.

De ongelijke verdeling van de warmteinvoer zorgt voor een ongelijke temperatuursbehandeling op verschillende plaatsen in de las. Op de hete plaatsen leidt dit echter tot korrelgrenssmelten en vervolgens scheurvorming uit deze gesmolten plaatsen. Dit ongewenste effect komt waarschijnlijk voort uit de gelijkstroomdoorvoer, die hoog is en niet constant maar een wisselend karakter vertoont. Dit kan leiden tot concentratie van de stroom in oppervlakten en turbulenties in de stroming (eddy currents).

Uitlijning en temperatuur zijn relatief makkelijk te beïnvloeden en dienen dus voornamelijk goed afgesteld te worden. De frequentie van de stroomdoorvoer kan aangepast worden zodat de turbulenties even groot zijn als het oppervlak van de las, maar bij oppervlakte geleiding kan het

echter zijn dat voornamelijk de grootte van de stroom de oorzaak is. Deze kan niet zo makkelijk beïnvloed worden aangezien een bepaalde warmteinvoer nodig is voor het lasproces.
De microstructuur van de las lijkt momenteel geen onneembare hindernis, aangezien lassen zijn gelegd met mechanische eigenschappen welke die van de basisplaat benaderen.

Abstract

In rim production a lower weight is desired. Therefore a new steel grade, with high strength and formability has been studied: HR45. In shaping the rim profile mechanical failure at the weld zone is a common feature. Two aspects of the process can cause this behaviour: the process itself does not have a good bonding as result or the weld microstructure is not as formable as the base material.

The weld process employs a current through abutting surfaces, which causes the metal to heat to the desired temperature by internal resistance. When this temperature is reached a axial force is employed to forge the surface together. In this process melting should not occur and is therefore called a solid state process.

In this research weld were made at different parameter combinations (weld force and current), to study the challenges in the process. The most important factors were the alignment of the steel sheets, the weld temperature and the uneven distribution of heat development (hot spots).

The alignment influences the final weld shape as well as the material flows during the forging action. Surface contaminants should be dispersed by the flows throughout the weld zone.

Temperature also influences these flows and should be chosen such that the material is softened. At lower temperatures the metal might be forgeable, but flows do not redistribute the contaminants properly, which become initiation points for crack forming. A weld temperature at which the material is softened and not only forgeable is desired.

The uneven development of heat employs different heat cycles in different places in the weld seam. In the hot spots intergranular melting and subsequent crack forming during forging can occur. This undesired feature originates in the current application but still two effects might cause this phenomena: the skin effect is caused by high current application which pulls the current to the surface and the alternating level of current can cause turbulent current flows (eddy currents). Which of these two or how these combine is not yet discovered.

The alignment and temperature are adjustable parameters so their influence can be altered. The frequency of the current application can be arranged to a point where the turbulences cross the total area of the weld zone, but when the skin effect is the determining factor, the value of the current is the limiting feature. It cannot be altered at random as a certain heat development is necessary for the weld process.

The microstructure does not seem a limiting factor in the process, since welds were made with comparable formability with respect to the base metal.

List of symbols and abbreviations

Symbols

Symbol	Unit	Explanation
A	m^2	Cross section of conductor
$C_{V,m}$	$Jkg^{-1}K^{-1}$	Specific heat at constant volume and mass
D	m^2/s	Diffusion coefficient
f	-	Emissivity factor
F	N	Force
h_c	$Wm^{-2}K^{-1}$	Conductive heat transfer coefficient
h_R	$Wm^{-2}K^{-1}$	Radiant heat transfer coefficient
I	A	Current
J	A/mm^2	Current density
HB_{RT}	HB	Brinell Hardness at room temperature
k	$Wm^{-1}K^{-1}$	Thermal conductivity
L	m	Length of conductor
m	kg	Mass
q	Jm^{-2}	Heat flux
Q	J	Energy
R	Ω	Total resistance between the clamps
R_b	Ω	Resistance of the bulk material between the clamps
R_c	Ω	Contact resistance of the abutting surfaces
R_{cl}	Ω	Contact resistance at the clamp-sheet interface
R_m	$Jmol^{-1}K^{-1}$	Molar gas constant (8.31 $Jmol^{-1}K^{-1}$)
t	s	time
T	K	Temperature
T_A	K	Air temperature
T_m	K	Melt temperature
T_{RT}	K	Room temperature (293 K)
T_S	K	Temperature of solid
T_v	K	Softening temperature
x	m	Length diffusion path

δ	m	Penetration depth of eddy currents
$\rho_{e,RT}$	$\Omega \cdot m$	Resistivity at room temperature
$\rho_e(T)$	$\Omega \cdot m$	Temperature dependent resistivity
ρ_0	$\Omega \cdot m$	Resistivity at absolute zero
ν	Hz	Frequency of weld source current
σ		Stefan Boltzmann constant
σ_e	$(\Omega m)^{-1}$	Electrical conductivity
θ_D	K	Debye temperature
μ_0	Hm^{-1}	Permeability of vacuum ($4\pi \cdot 10^{-7}$ Hm^{-1})

Abbreviations

AC	Alternating Current
BCC	Body Centred Cubic
CCT	Continuous Cooling Transformation
DC	Direct Current
DP	Dual Phase
FCC	Face Centred Cubic
FE	Finite Element
HAZ	Heat Affected Zone
HR	High Resistance
SEM	Scanning Electron Microscope
TEM	Transmitting Electron Microscope

1. Introduction

Wheel rim manufacturers as part of the whole automotive industry always look for ways to minimise the weight of car parts. In this instance stronger steel is selected for wheel rims, which can be made thinner, thereby limiting the weight. Rims are made from flat strips bent into a cylindrical form with the butt ends welded together. Finally the rims are rolled into a profile, which can hold the tire.

Resistance upset welding is the technique selected for butt welding rather than friction or flash butt welding, because of the short cycle time, safety and relative low energy consumption, and thus a more efficient heating [1]. This technique applies a current, I, through the interface between the abutting surfaces, which heats the metal locally to a forging temperature by Joule heating. Electrical resistance, R, in the set up (especially on the weld interface) obstructs the current, which has heat development, Q, as result. No melting should occur during welding, so it is classified as a solid state welding process. Applying a pressure that forges the material together performs the fusion of the two sides. Welding has been performed at Fontijne Grotnes with the Fontijne Holland Welder (Figure 1).

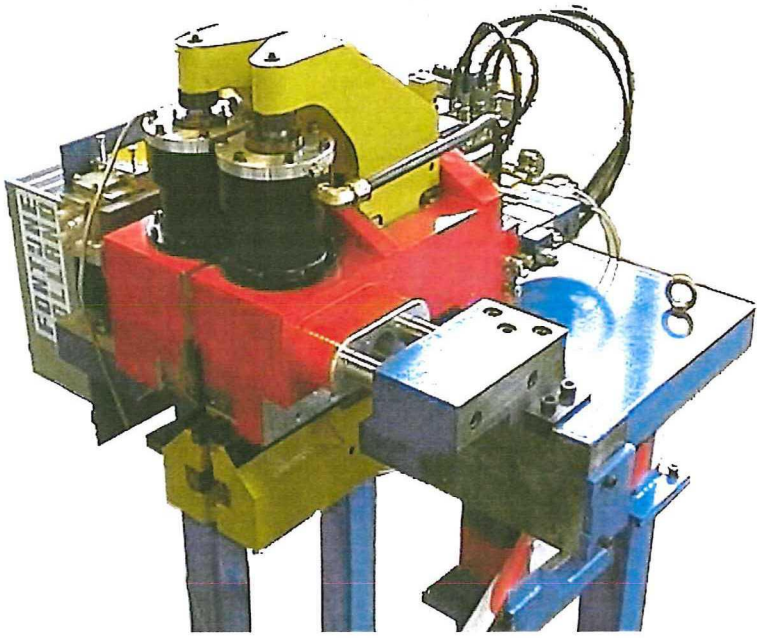

Figure 1: Upset butt weld apparatus: the Fontijne Holland Welder

Rim fabrication is a new application for the steel grade HR45, which has good strength and deformability. Mechanical properties are a result of the two-phase microstructure, which consists of a deformable ferrite matrix (grain size ~ 7μm) and strong bainite constituents (Figure 2). High formability also gives the name to this class of material: high resistance steels. These steels are low alloyed and their strength is purely a microstructural accomplishment.

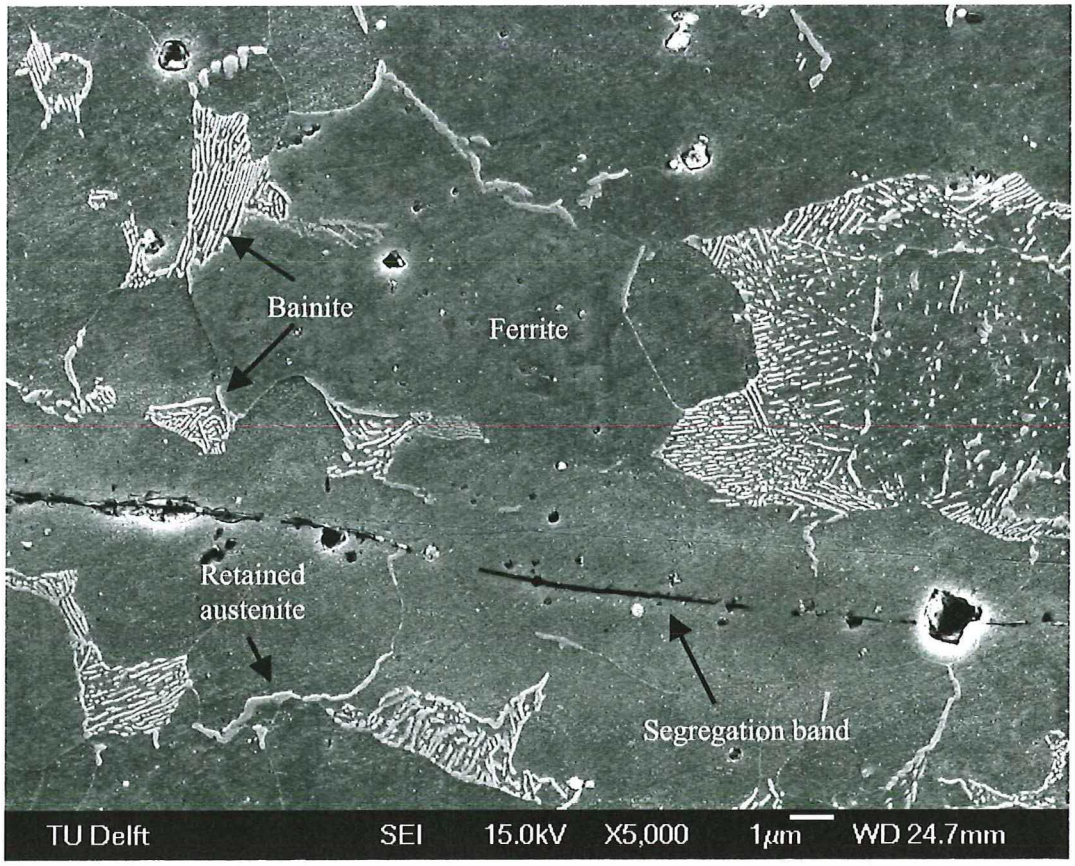

Figure 2: Base material in a welded sample, picture taken next to the weld

Welding these steels brings challenges from both an engineering and metallurgical perspective. On the engineering side the alignment and the application of the current cannot always be controlled to the desired level.

Metallurgical differences in the weld and peripheral zone result in an alteration in the mechanical behaviour compared to the base material. Although these changes may sometimes be severe, heat treatment during welding is adjustable and can be optimised until the mechanical properties are similar to those of the base material.

An extra feature of the material is the segregation band, which results from the rolling sequence. During welding this band undergoes a severe heat and mechanical treatment that can lead to specific failure when not controlled correctly. In Figure 2, the middle of the segregation band is visible as a black line, which is probably caused by etching the specimen; the segregation band itself is broader but has no definite borders.

In this thesis the main goal is to determine the nature of the poor formability in the weld zone. There are several features that can cause this behaviour: the forging action does not make a weld with desired dimensions, the surfaces may be incorrectly unified, leaving inclusions or pores that can cause failure on loading; the weld properties are not the same along the weld seam or finally, the microstructures obtained are too brittle.

All these aspects should be investigated, which is complicated by the weld sequence with all the available parameter combinations. Failure can be a result of the effects mentioned or of incorrect weld setup. By milling the weld surfaces a simplification is made; the interface will be cleaner and the contact resistance will vary less than when sheared samples are employed; this minimises the influence of the interface properties.

During the investigation the plates were not perfectly aligned, this was a constant and could not be altered. The influence will be mainly on the material flow in the forging action and as a result the weld shape deviates from that produced by a straight alignment and force application.

Alignment can thus have an influence on the bonding, as the surface contaminants can be trapped in the weld zone due to material flow. Bonding itself can also be altered by varying the heat input and the upset force as well as the upset distance.

In upset welding it is commonly acknowledged that at the sides of a sheet, an increase of the current density, J, can be observed, but this effect has a positive association for the welding process. It will be investigated whether this positive attitude can be maintained for the thin sheet welding of HR45.

Since the material is low carbon steel, hardenability is not expected to be very extensive and problematic. It is possible that the cooled clamps of the machine can, however, invoke such a cooling rate that hardened structures arise. Cooling of the clamps is necessary to prevent sticking and to cool the specimens to a temperature where the joint develops sufficient strength.

To investigate all these parameters welds were made and analysed in terms of weld geometry measurements, mechanical properties and microstructure. A qualitative description is made of the welding process with the features involved and finally some alterations to the process are recommended.

2. Theory

Chapter 2 covers the theoretical background of the process of upset butt-welding of HR45. Resistance upset butt-welding comprises of three stages: heating, forging and cooling. Each has its own influence on the final weld and material properties and all will be described in the first section. With this knowledge and the material properties, the material response for each step will be predicted globally in the second section.

2.1Upset butt welding

Resistance welding applies current through an interface with higher resistance, such that Joule heating in combination with pressure causes the materials to join. In most resistance welding techniques like spot and flash welding, the material becomes (at least partially) fluid and solidifies to form the joint. In resistance upset-butt welding, the material remains solid and the temperature rises above the forging temperature enabling the material to bond with a forging action [2].

Controlling the rates of heating, deformation and cooling is a complicated matter and has been studied and improved in other research [3], it will not therefore be a major topic in this thesis. Although some features of the control have an influence on the welding process, mainly in terms of decreased repeatability, control is still considered good or repeatable enough to investigate material response. Care should be taken in evaluating experiments, to be able to compare different specimens objectively.

Under production conditions, cooling is a result of radiation and conduction to the colder environment, which consists of the air and water-cooled jaws respectively. Control exists mostly out of changing the amount of material in between the jaws or the electrode temperature [4], but the rate of cooling can be further decreased by applying a gradually decreasing current [5]. Cooling occurs throughout the welding process but will be discussed separate from the heating to distinguish different heat flows.

At the end of the section an overview sketch is made of the total energy flow with a possibility to form a physical model for temperature calculation [6].

2.1.1 Heating

The goal of this step is to heat the metal to a temperature at which it can be forged, resulting in a solid-state fusion. Current, I, is applied through the interface is indicated by the red arrows in Figure 3. Although the Joule heating creates the majority of the heat, phase transformations and deformational heat also contribute to temperature changes [7, 8]. The current is an AC waveform that is converted to DC, with an inherited oscillating component (frequency ~1000Hz, amplitude ~ 2 kA, which corresponds to 10 A/mm^2) from this conversion. Control is actually performed by calculating the energy dissipation Q ($=I^2R$). The current is therefore a result of the given power input and the potential difference or more precisely, the resistance R between the jaws.

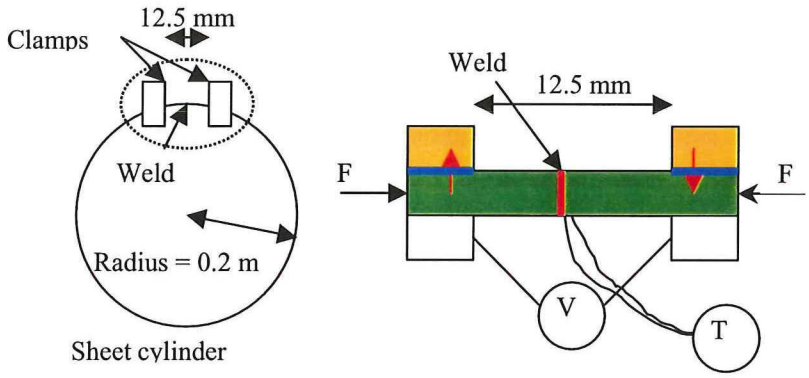

Figure 3: Welding set up, left the rim welding set up, at the right hand side an enlarged view of the clamps and weld zone, which is indicated by the dashed oval in the left hand side picture

Resistance is a cumulative combination of the contact resistance between the jaw (orange) and the plate R_{cl} (2x) (blue lines in Figure 3), the bulk resistance of the plate itself, R_b (green), and the contact resistance of the interface where the abutting surfaces touch, R_c (red line) (equation 1) [9]. Another resistance is the parallel bulk resistance of the sheet cylinder, but this will be absent during our experiments. Normally this resistance is higher than the resistance between the jaws, because the length of the rim is two orders of magnitude greater than the part in between the jaws (1.5m in comparison to 12.5 mm). The rest of the electrical circuit is made of thick copper with a sufficient surface area to minimise Joule heating.

$$R = R_c + R_b + 2R_{cl} \qquad (1)$$

R_b can be calculated by $\rho(T)L/A$, with $\rho(T)$ the electrical resistivity as function of temperature, L the distance in the plate along which current is conducted and A the surface area of the cross section. Calculating the contact resistances R_{cl} and R_c is harder and depends on several factors.
At the contact area between the plates and the jaws, the surface is large compared to the abutting surfaces and pressure can further decrease the resistance, R_{cl} should be significantly lower than the other two resistances combined (R_c+R_b), to prevent sticking to the electrode. To promote this, the electrodes are cooled and will remain relatively cold throughout the welding cycle. This has as a result that the heat transfer is always in the direction to the clamps, but the energy that is released can decrease the temperature gradient perpendicular to the weld seem.
Contact resistance between the plates, R_c, should then be the greatest factor in the composition of the resistance. A theoretical quantitative approach has been constructed and summarised by several authors [1, 10-13]. A more qualitative description will be given here to give an understanding of the process.
At the beginning of the welding process the surfaces are placed against each other. The surfaces are not completely smooth and will have only a limited number of contact points. Pressure can be applied to increase the number and total area of these contact points and decrease the resistance. Oxidation products on the surface determine what fraction of the contact surface makes electrical contact. At a certain deformation these oxides are broken and there will be a significant increase in contact area and thus a decrease in contact resistance, this will only occur after initiation of the upset. Contact resistance is at all times higher than the sheet resistance, R_b, and will have a higher local heating as result. This dependency is shown in a formula developed from a simplified model by Zwolsman [11]:

$$R_c = \frac{\rho_{e,RT}}{2}\sqrt{\frac{\pi \cdot HB_{RT}}{F}\cdot\frac{T_v - T}{T_v - T_{RT}}}\cdot\frac{T}{T_{RT}} \qquad (2)$$

In this equation, $\rho_{e,\,RT}$ is the electrical resistivity at room temperature [Ωm], HB_{RT} the Brinell hardness at room temperature [HB], F the force [N] and T_v, T_{RT} and T respectively the softening, room and actual temperatures [K]. Distinction between the forging and the softening temperature is that the first is actually a set of conditions where the atomic bonding due to diffusion is possible, while the second is a material property. The main conditions for forging include the stress, which brings atoms closer together and the diffusivity that is controlled by the temperature. These conditions are similar to diffusion welding, except that during upset welding deformation is

allowed [14]. The combination of temperature, pressure and deformation raise the suspicion that recrystallisation or grain growth might be a significant part of the bonding system.

An assumption is that at the same force and temperature, the area that makes actual physical contact is always equal, while surface roughness can also change this area. Even if this assumption is true, contact resistance can still vary significantly with the percentage of metallic surface. Especially at low stresses, where the total contact area is small, the role of surface conditions increases.

At temperatures greater than the Debye temperature, θ_D, the temperature dependence of the resistivity may be approximated by a linear relation [15], see equation 3. Since the Debye temperature for pure iron is 460 K, this is only valid for part of the welding process. Below this temperature the function for the resistivity switches from

$$\rho_e(T) = \rho_{e,RT}\frac{T}{T_{RT}} \qquad T>\theta_D \qquad (3)$$

to

$$\rho_e(T) = \rho_0 + A\cdot T^5, \qquad T<\theta_D \qquad (4)$$

where $A=\rho_0/5T_{(RT)}\theta_D^4$ if continuity is assumed at the Debye temperature. This transition originates from the amount of wavenumbers that are added by increasing the temperature. Below the Debye temperature. To be able to calculate what temperature change will be inflicted at a certain heat input, the molar heat capacity as a function of temperature is necessary. When the temperature increases the specific heat stabilises from

$$C_{V,m} = 9R_m\left(\frac{T}{\theta_D}\right)^3\int_0^{\theta_D/T}\frac{x^4e^x}{\left(e^x-1\right)^2}dx \qquad T<\theta_D \qquad (5)$$

to

$$C_{V,m} = 3R_m = 24.9JK^{-1}mol^{-1} \qquad T>\theta_D \qquad (6)$$

where $C_{V,m}$ is the molar specific heat at a constant volume, x is θ_D/T and R_m the molar gas constant [15].

On heating the resistance will change in two ways: first the resistivity of the material rises due to greater atomic vibrations (phonon-electron interaction). Secondly the contact resistance will decrease as the material becomes more deformable at a certain temperature (forging temperature; see equation 2). Contact points flatten more easily at the same applied pressure, the surfaces will get closer together and create new contact points. Both effects cause a decrease in contact resistance.

The joint line will continuously have the highest resistance and the highest heat development, whether this is a result of contact resistance or increased resistivity. Temperature can be calculated when the energy that is released as heat is divided by the specific heat.

A feature that can arise during upset butt welding is the creation of hot spots, *i.e.* places where the interface heats up faster than the rest of the weld seem. Often these spots arise a small distance from the weld seem ends. Four potential explanations have been found that can describe the existence of these spots, but none has found sufficient theoretical or experimental support. First the application of the current is not necessarily distributed evenly along the weld seem length. It is possible that due to the passage of the current from the copper circuit to the plates, converging of the current taken place, as the plate is smaller and has different electrical properties.

The second explanation is due to heat reflection by the surface; especially at the sides of the weld seem, there should be increased heat reflection. Not only can the heat redistribute at the upper and lower side, but also at the weld seam end.

Thirdly, when the clamping pressure applied is not straight on the plate surface, but next to the plate, the electrode might bend around the plate, resting on the edges of the plate, leaving an air gap in the middle. Electrons will then only flow in and out of the material via the sides [16].

The last option comes from the theory that electrons favour edges as excitation locations, when such an edge is present in the set up, the flow pattern of the current is influenced [17, 18].

2.1.2 Forging

When the forging temperature has been reached, the abutting surfaces are pushed together along a certain distance, the upset distance. This movement forges the material together and pushes some material aside, the displaced material is called the upset. Surface contaminants can be trapped in the weld zone, as it stays solid and can only partially flow out with the upset. Further the material is highly deformed, up to 40% at a mean deformation rate as high as 0.8 s^{-1} and at a maximum of 2 s^{-1}.

The flow pattern of the material depends on the applied force, the temperature (or rather the extent of softening) and the alignment. From the threshold deformation that is needed to break the

oxide layer, the interface can start to move outwards. If this value is not reached, the oxides keep the base material together and an improper weld will be obtained [12]. For breaking of the layer at room temperature a deformation of up to 70 % (in zinc) is needed [19]. Oxide film fragments are spread through the weld as the material deforms. Although earlier it was assumed that these fragments could be transported by the metal flow to the upset, leaving no oxide in the weld metal, this was contradicted by Nied [20]. Oxide particles are only spread throughout the weld in the way spots on a balloon spread as the balloon is blown up.

Above the softening temperature the material deforms quickly, but the rate of deformation should not be especially temperature dependent, as above the softening temperature, the material would deform at any level of stress. Therefore the amount of stress applied should be the main influence for the deformation rate. Especially because the process is not an equilibrium situation, inertia of machinery can cause a lower deformation than would be expected at the measured temperature. Closer to equilibrium heating the transition will be easier to spot due to greater deformation at certain temperatures. During the heating there is more time to deform, while at high heating rates the temperature has already been raised before the material had a chance to deform. In general terms: the kinetic process of deformation cannot keep up with the thermal effect of softening.

Alignment in the welding process is theoretically straight (Figure 4a), but achieving this may not be straightforward. The electrodes often wear, giving room for misalignment and the application of pressure can also be uneven. Different modes can be found for varying directions of misalignment, each causing different weld shapes (Figure 4 b, c and d).

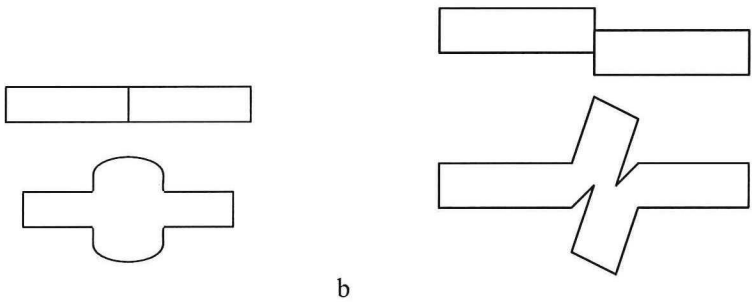

a b

Figure 4: Possible alignments and weld forms: a) is a straight alignment, b) plates are shifted

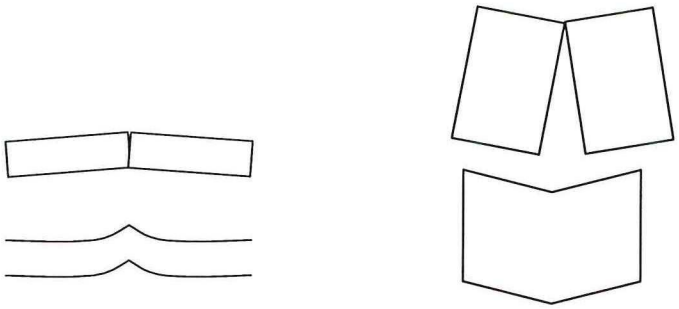

c d

Figure 4 (continued): c) an angle in the front view and d) an angle in the view from above

Finally the segregation band will also be deformed during upsetting. Flow patterns have been calculated with finite element methods and an example is shown in Figure 5. In the middle of the plate thickness where the extension of the segregation is maximal, outward flow is minimal, so it is possible that the band of high content of solute elements is folded together and even more concentrated at the weld interface. Another possibility is that when the upset force is not aligned, the band is bent and will flow into the upset (Figure 4b). After removal of the upset, the segregation band reaches through the surface and can make it a favourable spot to initiate cracking or corrosion [21].

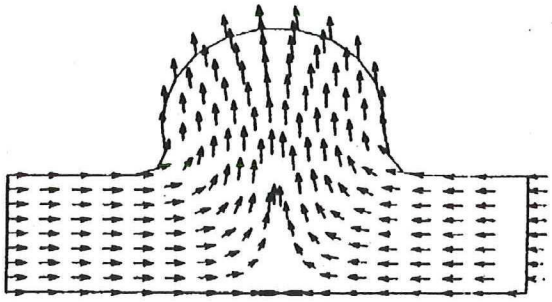

Figure 5: FE model of a possible flow pattern in upset butt-welding [20]

2.1.3 Cooling

The stored heat will be radiated and conducted away from the weld zone. Only a small shrinkage will occur from the cooling. The cooling rate is determined by the heat capacity of the jaws (how well they are cooled), the distance along which the heat has to be conducted, the free surface that can radiate and the temperature difference between plate and surroundings and is given by [22]:

$$h_R = \sigma \cdot f \cdot \left(\frac{T_S^4 - T_A^4}{T_S - T_A} \right) \qquad (7)$$

in which h_R is the radiant heat transfer coefficient [$Wm^{-2}K^{-1}$], σ the Stefan Boltzmann constant, f a factor that is dependent on the emissivity and surface dimensions and T_S and T_A the respective temperatures of the solid and air [K]. The heat transfer by conduction can be limited by two factors: the heat conduction along the plate or the heat transfer from the plate to the jaw. The theoretical approach of the latter is regarded as too complicated for practical appliance and only a very general equation with empirical parameters has been found (equation 8) [22].

$$h_c = \frac{q}{\Delta T} \qquad (8)$$

h_c is the heat transfer coefficient of the contact interface, q the heat flux through the interface and ΔT the temperature difference between the clamps and the workpiece.

The basic equation (equation 9) for heat transfer by conduction in a plate is limited by the conditions that the temperature difference is small so temperature dependency of the conductivity is not included [22]. Radiation is also excluded from this equation, which lowers the effective heat transfer by conduction as not all heat has a chance to be conducted to the jaws but is partially radiated.

$$q = -k \frac{\partial T}{\partial y} \qquad (9)$$

q is the heat flow per unit area, k the materials thermal conductivity and y the distance between the hot and cold area. Below θ_D, k can be approximated by

$$\frac{1}{k} = \alpha T^2 + \frac{\beta}{T} \qquad (10)$$

where α and β are material constants [15]. Above the Debye temperature, the sum of electron and phonon conductivity is very material dependent (*e.g.* phase changes influence the phonon interaction) and a generalisation has not been found. Empirical data can be used to calculate temperature changes in these ranges.

The temperature gradient in upset butt welding is too high to fulfil these conditions, making the thermal conductivity a temperature dependent factor and adding a radiation component. These adjustments make the system complicated, especially with the transition at the Debye temperature, and more suitable for a Finite Element calculation.

The temperature of an increment can be calculated throughout the process by subtracting the total cooling from the total amount of energy that is dissipated into the weld zone and divide it by the specific heat. As the heating is intentionally higher locally on the weld zone, all energy inputs and losses are temperature dependent and the temperature is a function of location. In Figure 6 an increment is shown which receives heat from

- Heat conduction from the weld interface (green arrow), Q_w
- Heat development by Joule heating or phase transformations in the increment, Q_b

and rejects heat by

- Radiation to the environment (red arrows), Q_r
- Heat conduction to cooler parts nearer the clamp (blue arrow), Q_{cl}

When all these heat fluxes are added up the temperature change for the increment can be calculated from the remaining heat or the energy that is withdrawn. In an energy balance (adapted from Cacciatore [23]) this would be:

$$Q_w + Q_b - Q_r - Q_{cl} = \Delta T \cdot C_{V,m} \cdot m \qquad (11)$$

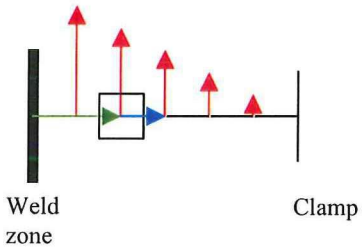

Figure 6: Heat flow at a specific place in the weld zone

2.2 Microstructural development

The base material consists of ferrite and bainite as stated before. The ferrite has grown within the austenite-ferrite intercritical area conditions of the phase diagram (between A1 and A3 in Figure 7) [24-26]. The equilibrium carbon content (max. 0.02 wt%) at these temperatures (723-900 °C) is higher than that at room temperature (0.008 wt%), but still it is lower than the overall carbon content of HR 45 (
Table 1) and therefore carbon will diffuse to the remaining austenite that is not yet transformed [26-28]. Due to the carbon enrichment in austenite and an elevated cooling rate after the ferrite forming, bainite is formed. Phase diagrams do not explain the meta stable phase forming during quenching, so an additional Continuous Cooling Transformation (CCT) diagram is needed. These diagrams describe the behaviour of phase forming during non-equilibrium cooling conditions. Sheaves and the laths and carbides within are visualised in the base material by means of a Scanning Electron Microscope, indicating the presence of bainite (Figure 2). Optical microscopy did not give conclusive results concerning the identity of this phase.

Table 1: Composition of HR45 in wt% as determined with optic emission spectrometry [29]

C	Si	Mn	P	S	Al	Ti	Nb	V	N
0.14	0.01	0.7	0.015	0.007	0.04	<0.001	<0.001	<0.001	<0.002

High resistance steels are sometimes classified as Dual Phase steels, and although there are great similarities in structure and production, reaction to deformation can differ. Dual Phase steels exhibit continuous yielding while High Resistance steels have a distinct yield point. Moveable dislocations, which are not bonded to carbon, are brought into DP steel by martensite formation.

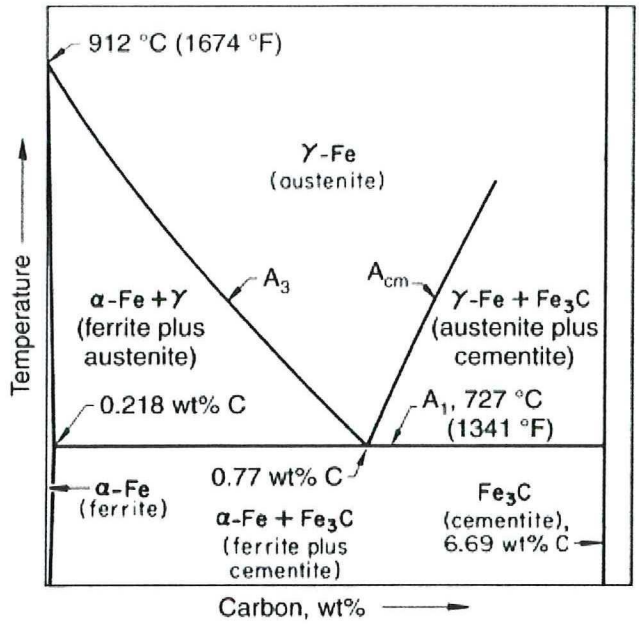

Figure 7: A part of the iron carbon diagram [30]

Another theory has been developed which states that the internal stresses, caused by martensite formation, help the initiation of yielding. After this the material can absorb deformations by moving the free dislocations [31, 32]. Dislocations do not have to be brought into the material, causing the missing of a yield point. In hot rolled steels like HR 45, the dislocations can move after deformation and be pinned by carbon. HR steels therefore have less free dislocations and will show a specific yield point at the stress level where dislocations are formed.

Microstructural changes are induced by the three steps (heat input, forging and cooling) described in the previous section. Each step has its own influence on metallurgy and these are presented separately for clarity.

2.2.1 Heating

At first heating (up to 600 °C) the material can exhibit processes that are related to tempering, *i.e.* increased recovery, carbide formation, austenite decomposition and aging. Bainite forming at any temperature includes the autotempering effect of increased recovery, relative to martensite forming [27]. Bainite in the base material is upper bainite and has been formed at relatively high temperatures, leaving small quantities of carbon in solid solution. Deformations applied to the

material are relatively scarce after the hot rolling and bainite forming, and will limit the extent of the first process of increased recovery.

Carbides in the bainite can only dissolve at higher temperatures and, in contrast to martensite will not cause softening due to the forming of carbides from solid solution. As the carbon already precipitates and the carbon content in the ferrite is low after intercritical ferrite forming, carbide formation is not plausible [27].

Decomposition of austenite can only occur in small quantities, for there are only small amounts of residual austenite after intercritical ferrite forming and high temperature bainite creation.

An effect that can soften the structure is the transition from ferrite plates into equiaxed ferrite, although the mechanism and driving force for this process are unknown.

Over 700 °C, the ferrite bainite structure begins to transform to austenite. During this process of transforming to a fully austenitic structure, carbon is redistributed through the material. Also the material softens as a result of the phase transformation and higher temperature.

2.2.2 Forging

Upsetting is the action of forging the surfaces together, in this action a lot of dislocations are brought into the material. Recovery will occur at elevated temperature (>400°C, [33]), but recrystallisation is a more favoured process in austenite to remove dislocation stresses [33-36]. In austenite stacking fault energy is relatively low, causing only a small amount of stress, and cannot deliver the driving force for recovery. Although at high temperatures diffusivity of atoms as well as dislocations is enhanced, reconstructive recrystallisation with dislocations as nucleation points is faster.

Neither dynamic nor static descriptions of recrystallisation suffice for upset butt welding, since these models describe the process by continuous deformation and recrystallisation from a cold deformed material. A system called meta dynamic recrystallisation can describe the conditions for deformation involving one deformation at elevated temperature. The nomenclature springs from dynamic nucleation, where the growth of the grains occurs without additional straining [37].

2.2.3 Cooling

Heat is extracted from the weld by radiation to the environment and conduction to the water-cooled jaws. All flows are directed by temperature gradients that decrease upon cooling. The cooling is then relatively continuous, except for the phase transformational energy that is released, which gives a decrease in cooling rate.

Phase transformations upon cooling to ambient temperature can be predicted from the CCT diagram. A cooling rate and a composition can give enough information to estimate a phase composition from a CCT diagram with the program viewCCT [38], which is shown in Figure 8.

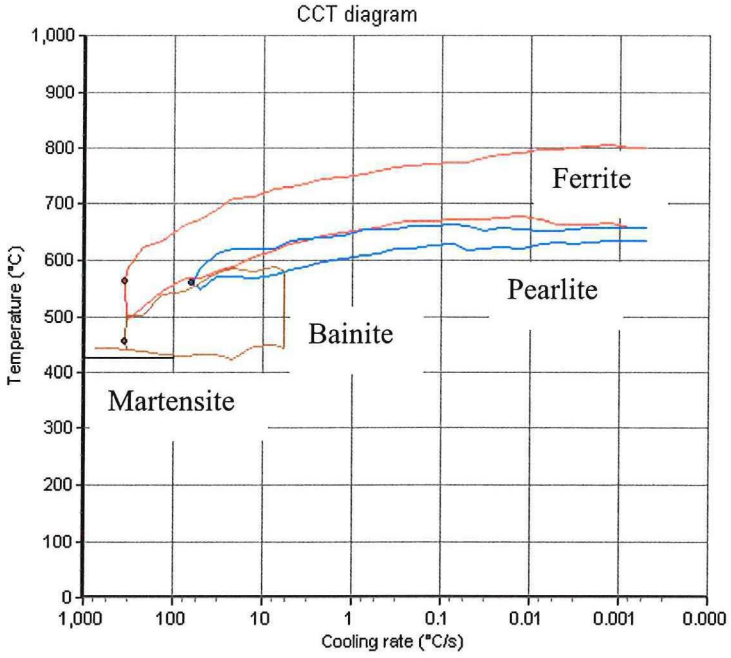

Figure 8: A CCT diagram for HR45, calculated by viewCCT [38]

A mixture of ferrite and bainite is predicted with a cooling rate between 70 and 200 °C/s, which are credible values in this welding process. The austenite is considered to have a flat concentration profile, although some variations will be present, which can cause slight changes to the CCT diagram. An increase of carbon will shift the forming temperatures upwards. At first ferrite is formed at a high rate from the austenite grain boundaries in plate morphology which is called a Widmanstätten structure [39]. Carbon partially diffuses into the austenite in front of the ferrite crystals, and can also form carbides between the plates.

The remaining austenite has an increased carbon content which is necessary for the formation of bainite [27]. Due to the high cooling rate, not all carbon has time to diffuse and form interlath carbides, some remains partially within the ferrite laths and forms small intralath carbides, which are associated with lower bainite. Bhadeshia [27] states that a carbon content of at least 0.32 wt% is needed to form lower bainite, so if the ferrite is depleted to 0.02 wt% percent, 0.12 wt% is

diffused to the grain boundary carbides and into the austenite. The ferrite volume has to be at least 60% to induce the forming of lower bainite.
The new structure is often less deformable than the base ferrite matrix, because of the interplate carbides in the Widmannstätten ferrite and the lower ductility of lower bainite in comparison with upper bainite. On the other hand, this structure may have a changed ferrite grain size, which is larger due to austenite grain growth during welding.

A feature that has been observed in low carbon steels is the hot embrittlement of the intergranular regions [40]. These are often enriched in sulphur, which lowers the melt temperature. In the welding process this melting temperature is exceeded and will melt, leaving crevices in the weld zone as there is no fluid weld metal to fill the cracks. When pressure is applied, cracks up to several hundreds of micrometers length can be formed.
Although this embrittlement should only occur at high temperatures, which should not be employed during welding, hot spots (uneven heat development) are sometimes present, which have a higher temperature than the rest of the weld seem. Thus the embrittlement is a feature that occurs due to incorrect welding and should be avoidable.

3. Experimental procedure

In general two types of experiments have been performed, plain welds and specific (Gleeble) experiments to exclude different influences and focus on one or two parameter influences. Plain welding has been executed with a range of parameters and subsequent mechanical testing and microstructural investigation has been performed. The main goal is to determine the parametric areas where welding is acceptable, those that exhibit a certain behaviour that causes the weld to be insufficiently formable and to be able to explain this behaviour. Gleeble experiments were performed to show clear influence of temperature cycle on microstructure or measure temperature depending material features.

Both type of experiments demand further analysis by standard techniques like formability, hardness and optical microscopy. Additional analysis with a Scanning Electron Microscope and ultrasonic evaluation will also be performed where necessary. These techniques will be described in section 3.3.

3.1 Plain welding experiments

For the welding experiments a test set-up has been built by Fontijne Grotnes, the Fontijne Holland Welder. It was built to simulate the welding of rims, especially to optimise control of the computer program. Plates with a cross section of up to 600 mm^2 can be welded at a current density of 100 A/mm^2. A separate AC/DC converter delivers the current (black arrows in Figure 9), which is controlled such that the delivered current is always 70% of the requested current. The current is applied through the upper side of two jaws that are made of a wear resisting, conducting copper alloy (upper blocks in Figure 9). These jaws clamp the sample and conduct the current, therefore care has to be taken that the electrodes do not stick to the specimen due to local heating on the jaw-sample interface. This is achieved by cooling the electrodes. Current is applied in the rolling direction of the steel sheet.

Clamping force is generated by two hydraulic cylinders that control the lower half of the jaws, which do not conduct welding current (lower blocks in Figure 9). Only a negligible current, that is used to measure the potential difference between the clamps, runs through the lower jaws. It was assumed that electrons would not cross the jaw-plate interface twice, while the main electrical field is in the direction of the other jaw.

Upset force is created with a hydraulic cylinder by an arm that holds the right hand side jaw, indicated by the red arrow in Figure 9. Due to the length of the arm, force may not be totally perpendicular to the weld interface, leading to an asymmetric weld shape as shown in Figure 4. Rims were not welded, so an alteration is that there is no current through the sheet cylinder, but only passes through the abutting ends of the sheet.

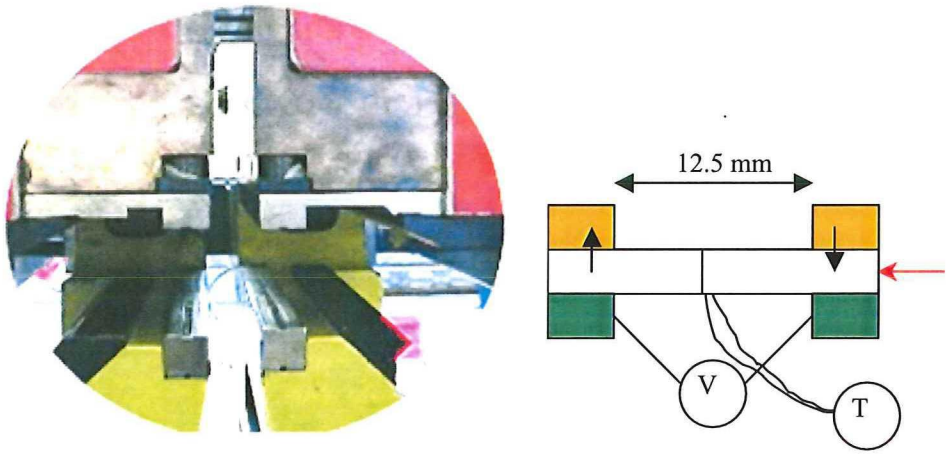

Figure 9: Weld and measuring set-up

Dimensions of the sheet in the experiments performed were a 60×75×1.6 (l×w×h) and 12.5 mm gap opening distance (interface in the middle so 6 mm from each clamp). The 75 mm wide butt ends were welded together.

K-type thermocouples of 0.25 mm in diameter and a delay of 0.34 seconds were spot-welded on the desired places for temperature measurements. Temperature was recorded as a DC measuring signal by an Agilent 34970A data logger with a 16 channel 34902A measuring card. A calibration has been made to calculate the temperature from this data. Sampling speed of the data logger was 100 Hz in total, so the sampling speed of a single thermocouple is 100Hz divided by the number of thermocouples.

Voltage, current, force and displacement were recorded as a function of time by the welding equipment. The measured potential difference between the lower jaws consists of the same three parts as the resistance in the theory chapter: two times the jaw-sheet contact resistance, the sheet bulk resistance and the sheet-sheet contact resistance. Although this combined measurement cannot be split into separate parts these measurements can give qualitative information on the temperature and contact resistance, which are related. The potential difference rises with

increasing temperature due to increased resistivity and when the contact resistance is stopped this barrier loss should be visible as a potential difference drop or change in slope. But as the specific resistivity is not linear with temperature and the contact resistance can gradually disappear, this evaluation is complicated and dependent on the extent of the effect.

The measurements of the current can mainly be used for the calculation of the heat input. Multiplied with the voltage the total power that is dissipated into the weld is extracted. This also includes the heat that is developed at the jaw-sheet interfaces.

The pressure in the upset cylinder was taken as a measure of the pressure exerted. Force can be calculated by multiplying the cylinder pressure and the cylinder surface area, which is approximately 2000 mm^2. The force is a controlling parameter, but sudden changes (increase) in deformability in the material will be visible here as a result of the inertia of the machine.

Displacement (and its derivative speed) measurements indicate the extent of softening and are used as a condition between different program steps. Initial movement will be fast as the interface is softened extensively. As the upset continues, colder, harder material will be pushed into the weld, decelerating the apparatus. This retarding of the upset movement can be avoided by increasing the current to such a level that during welding the peripheral zone will be hot enough and during the whole upset movement softened material will be deformed.

Welding was computer controlled. The computer program that controlled the apparatus consisted of five steps, with an example given in Table 2:

- Gap closing (apply force to ensure contact at the interface)
- Heating (heat the material to forging temperature)
- Yielding (forge the sheet ends together, while continuing heating)
- Curing (cooling and application of force to keep the weld together while cooling)
- Exit phase (release of the specimen)

Table 2: Instance of a welding program

Step	P [MPa]	J [A/mm^2]	dx [mm]	dt [ms]
Gap closing	70	0	1.0	100
Heating	80	100	0.3	2000
Yielding	100	100	5.0	2000
Curing	40	0	1.0	100
Exit phase	10	0	1.0	10

The second and third two columns contain the values that the apparatus should deliver in that step during the process. The last two columns contain the restrictions for the end of a step. So if for example in the yielding step the displacement is 5.0 mm the following step is initiated. When 5 mm is not reached, the welding continues for 2000 ms before continuing with the next step. The total time of the progress was limited to three seconds in order to prevent overloading of the current source. The choice of the time or upset limits obviously depends on the step; in the first step only a given force has to be exerted on the material, which takes a small amount of time, while the upset limit must be relatively high to enable the machine to close all the existing gaps. The second limit has a more sensitive touch as it chooses between the softening of the material and the limits of the power supply. At 0.3 mm upset it is considered that the upset speed is increasing as a result of the forgeable metal, indicating it is the right time to start upsetting. When this step takes more then 2 seconds the chance of overstretching the capabilities of the apparatus increases. Therefore the step length is limited to 2000 ms the same as in the upset step, while the whole program can only last for 3000 ms. As a second consideration the required cycle time for the fabrication of wheel rims is also exceeded. When the metal is soft enough the upset distance will be reached in the third step. The last two limits are set to give the specimen some time to cool, but due to the decreased pressure, which is intended to hold the weld seam together, deformation should be small enough not to deform the weld.

Parameters which have with their own reaction in the process and were varied in the experiments were the:

- Upset distance (3 and 5 mm)
- Clamping force (50-80 MPa)
- Upset force (70-100 MPa)
- Current density (70-140 A/mm^2)
- Interface properties (sheared or milled)

Upset distance is determined by the deformation that is needed to bond the surfaces on an atomic scale. It is estimated that below 3 mm upset, surface contaminants are not dispersed enough through the weld seam and these will weaken the bond extensively. Above 5 mm upset distance the upset would become too large and possibly stick in between the two clamps to the electrodes. Also, the material losses would be too extensive while not adding advantages to the weld quality. Clamping force is chosen around 20 MPa under the upset force, to ensure contact throughout the process and to indicate the start of the softening to trigger the next step of upsetting. The base upset force (100 MPa) is an empirical value that has found reasonable results in tests with other

materials, and the other values are adjustments to cover a broader spectrum of parameter values when the base value appeared too high for HR45. Current density choice is based on the same principle as that of the upset force. Two attempts at higher and lower values (140 and 70 A/mm^2) have been executed in preliminary experiments and while the first gave melting, the second had no bonding at all.
The effects of interface properties where also roughly examined during these preliminary tests, and because of the lack of conclusive information, the process was simplified and the factor of irregular surfaces excluded as much as possible by milling the abutting surfaces of the sample. This will make comparing a theoretical approach with the experiments easier and the results of the experiments more consistent.

For each parameter combination at least three specimens were welded, when the welds did not match after visual inspection, up to two extra specimens were welded. For statistical purposes this is too small a number, but for the purpose of detecting the difficulties within the process, it is suitable.
A number of plates without joint interfaces were positioned in the welding apparatus to check whether current distribution is an effect of the machine or whether pressure differences at the interface cause a resistance decrease. Welding parameters were a contact and heating pressure of 50 MPa, upset pressure of 70 MPa and an upset distance of 3 mm. Current density was varied between 80 and 100 A/mm^2.

3.2 Specific experiments

Some features of the material or the process could not be observed during welding because there were too many disturbing influences and the program could not control parameters such as temperature and deformation. Three experiments have been performed on the Gleeble to exclude these factors. First the influence of a heat cycle comparable to the welding cycle on the segregation band was examined. Secondly an approximation for the austenitisation temperature and speed was made and the last experiment involved the determination of thermo-mechanical conditions where the material can be forged. Experiments were performed in low vacuum and a schematic drawing of the samples can be seen in Figure 10.

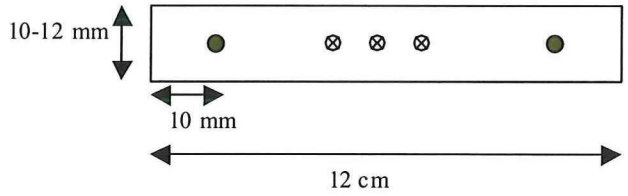

Figure 10: A specimen used for the determination of the homogenisation of segregation bands [41]

Two thermocouple arrangements where employed: only one thermocouple and three thermocouples. The black dots are holes with a diameter of 5 mm to fix the specimen and the encircled crosses are K-type thermocouples (from left to right TC2, TC1 and TC3). The middle (TC1) also gives feedback to the Gleeble to control the temperature.

In the one-thermocouple experiments the thermocouple is placed in the middle of the specimen. In the three-thermocouple arrangement the additional two are placed at equal distances of about 10 mm on both sides of the middle. The wires of the same material (in thermocouples there are two wires from different materials, *i.e.* chromel and alumel) are placed at the same side (all perpendicular to the current) to prevent the thermocouples picking up potential differences due to the bulk resistivity of the lesser conductive part of the circuit (with a high electrical field) in the welding circuit. This should already be minimised by applying the current in pulses and measuring when there is no pulse. The frequency of the pulses is 50 Hz.

3.2.1 Segregation band dissolving

The first tests that performed were tests to measure the homogenisation of the segregation bands that are present in the delivered material (HR45). Therefore the specimens were placed in a Gleeble 3500®. Then the specimens were heated at two different rates to 1100 °C, held for varying times and subsequently be cooled.

The goal was to detect whether it is plausible that the segregation bands are dissolved and in which time during the welding process or if not, to what degree the dissolving is taking place. Because the heating only takes place around the weld, this will be a localised effect in welding.

The examination of the segregation bands was performed with an optical microscope, therefore the accuracy of microstructural quantification is limited.

Table 3: Used values for different parameters and number of thermocouples

Heating time to 1100 °C [s]	Holding time at 1100 °C [s]	# of thermocouples	Extra quenched specimen	x_{Mn} [µm]	x_C [µm]
1	1	3	yes	0.10	15
1	2	1	yes	0.12	19
1	5	1	no	0.17	27
2	1	3	yes	0.10	15
2	2	1	yes	0.14	22
2	5	1	no	0.18	29

The first parameter that was examined, was the upslope of the temperature. Two speeds were chosen. One is the maximum that can be generated by the machine, while it is still controllable. This was found to be 1100 °C per second. The other speed was half of the maximum: 550°C per second.
The program could not achieve this rate without an overshoot, so the program was altered to fit the heating cycle during welding and limit the overshoot.

The second parameter was the holding time. Short holding times (1 and 2 seconds) were chosen because they are more or less equal to the time that the wheel rim welds are at this temperature. Longer holding times were chosen to see when the segregation bands are really dissolved. The first time that is set for these experiments was 5 seconds.

The last parameter is the down slope of the temperature. Most specimens were cooled in air to simulate the cooling after welding. A few of samples were quenched to check whether the dissolving of the segregation continues during cooling. In these experiments the quenching device was aimed at the opposite side from the side where the thermocouple was placed, to avoid excessive cooling of the thermocouple.

During the experiments no pressure was exerted on the material to prohibit buckling. There are still two choices left: displacement or force control. The first keeps the displacement on zero, but then, due to heat expansion, a little compressive force builds up in the specimen. This force can

be measured. Otherwise the force can be set to zero to prevent stress in the material, and then displacement can be measured when it is significant. Force control was selected for the greater similarity with the welding process.

An estimation of the length of a diffusion path, x, can be calculated by the square root of the product of the diffusion coefficient, D, (temperature dependent) and the time, t, which the material spends at elevated temperature. These estimations for carbon and manganese are shown in Table 3 (respective diffusion coefficients at 1100 °C: $1.2 \cdot 10^{-10}$ [42]and $4.6 \cdot 10^{-15}$ m^2/s for a 0.35 wt% manganese [43, 44]).

3.2.2 Austenitisation speed

Normally heat-involving processes take enough time to transform all constituents to austenite. In this relatively short process full transformation is less certain. Knowledge of the dependency of heating rate and peak temperature can give a better insight into the metallurgy involved in welding. Especially the structure that is present before the upset is of importance as it is the initial situation for the next step of deformation. In addition to checking whether the transformation is complete, austenite grain size as a function of peak temperature can be determined.

To measure where the base material to austenite transformation is complete and the corresponding grain sizes, a series of experiments have been performed at two different heating rates to certain temperatures. Rates were 400 and 800 °C/s and peak temperatures were 650, 700, 800, 900 and 1000 °C, which should cover the whole austenite transformation range. After austenitisation, specimens were quenched with an atomised water spray.

It can be seen that at constant rates, heating to higher temperatures also involves an increase in time at elevated temperatures due to longer heating times. So two effects are combined, higher temperature and longer cycle times. These effects add up and the contrast between the steps should be larger, but the resolution in the transition area is small.

Another difference is that composition of phases is also dependent on the peak temperature. Noses in the CCT diagram will be crossed but at different rates or different composition of the phase formed.

3.2.3 Determination of forging temperature

Earlier it was assumed that the material temperature should be elevated to the softening temperature (2/3 T_m [°C]+273; [11]). Softening happens at the temperature where the material cannot take any pressure at all. Experiments showed that forging could already be performed at lower temperatures. Therefore a forging temperature should be determined.

Experiments performed were the heating of a strip to 1200 °C at two different rates (400 and 800 °C/s) and three different levels of stress (0, 50 and 90 MPa compression). Zero stress level was executed to be able to extract the temperature dependant features: phase transformations and extension caused by heat.

Deformation was determined as a function of temperature. When the deformation speed at a constant stress level increased suddenly, this was taken as the forging temperature. Further temperature dependency up to the softening temperature can also be determined by the deformation rate. From the statements above it follows that deformation is constant at increasing temperatures. Whether this is a correct assumption or not should be investigated.

3.3 Standard evaluation tests

Standard evaluation tests are necessary to be able to describe and compare different sample reactions to thermo-mechanical treatment. In this research project there were five different types of evaluation:

- A macro description of the weld, to be able to relate the dimensions and look of a weld to the mechanical properties
- Erichsen tests, to compare formability with that of the base material,
- Hardness measurements, to compare different zones in and next to the weld to the base plate properties,
- SEM evaluation, to identify phases and measure local compositions
- Optical microscopy, to compare different structures and interpret the origin of different mechanical behaviour

3.3.1 Macro description of weld seam

Mainly the dimensions of the upset were measured along the weld seem. When welds were evaluated and given a certain quality level, a search for the relationship between this level and the upset dimensions was made. Heat profiles can also be seen on the specimens because the material changed colour after release of the specimen, but these are harder to describe objectively or quantitatively.

Height and width of the weld seam were measured with a calliper every 7 mm (indicated by the scratches in Figure 11), which is one-tenth of the total plate width.

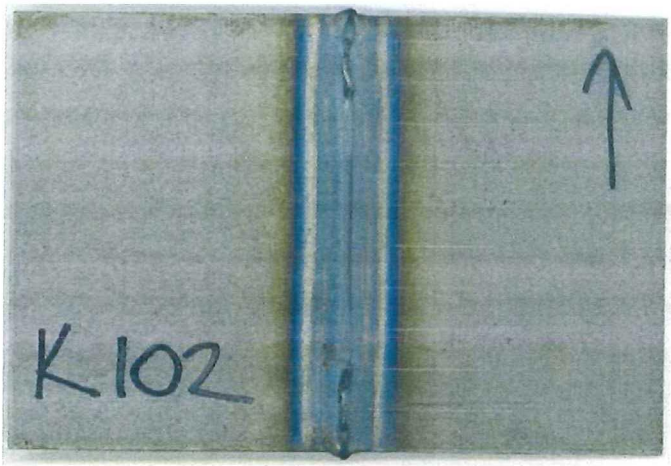

Figure 11: Picture of welded plates

Difficulties in measuring lie within the slope of the upset that gradually increases, lacking a definite boundary. In low current density specimens, where the upset distance was not obtained, upset dimensions could only be measured with a subjective judgment of the place where the upset began and finished. In the middle where temperature was lowest plates were sometimes only moved downwards, leaving a cleavage of which the height and width could not be measured accurately. Another feature is that at this distance between measuring points, some characteristics of the weld might not be represented, although the weld as a whole is described fairly.

3.3.2 Erichsen formability tests

The rims are cold-rolled to the shape of the rim after welding. These series of rolling actions (flaring and 3 to 5 profile rolling steps) require an extensive deformation. The materials themselves are highly formable, but the changed properties in the weld area can lead to cracking during roll forming. Therefore it is important to measure the formability of the weld. The elongation during tensile tests gives an indication of the formability. But to approach the type of deformation during the rolling process the Erichsen cup test was selected (Figure 12). A ball bearing is pushed into the plate at a constant speed until cracking occurs. When the crack becomes visible or when the force suddenly drops due to failure the machine is stopped. The depth of the indent at failure is a measure for the formability. Normally the form of the crack is circular (Figure 13a). When the weld quality is not sufficient, the crack grows along the welding line as can be seen in Figure 13b. To perform the tests, the upset on the upper and lower side had to be removed. In a production environment, this is done directly after welding with a set of

chisels. During this processing step, the chisels can tear extra material out and the material can also be deformed during chiselling and rolling. These treatments can work-harden the material or cause crack initiation points. In the test environment the major part of the upset is milled and as finish sanded smooth, and especially the sanding can cause heating of the weld zone, but minimal deformation. Creating the smooth surface can have as a result that the plate is slightly thinner than the original thickness. Care has to be taken that the upset removal does not cause heating of the plates, which will inflict changes to the microstructure.

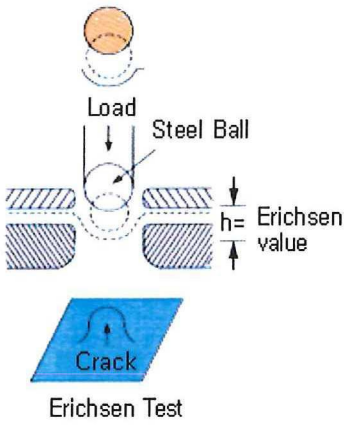

Figure 12: A schematic drawing of the Erichsen cup test [45]

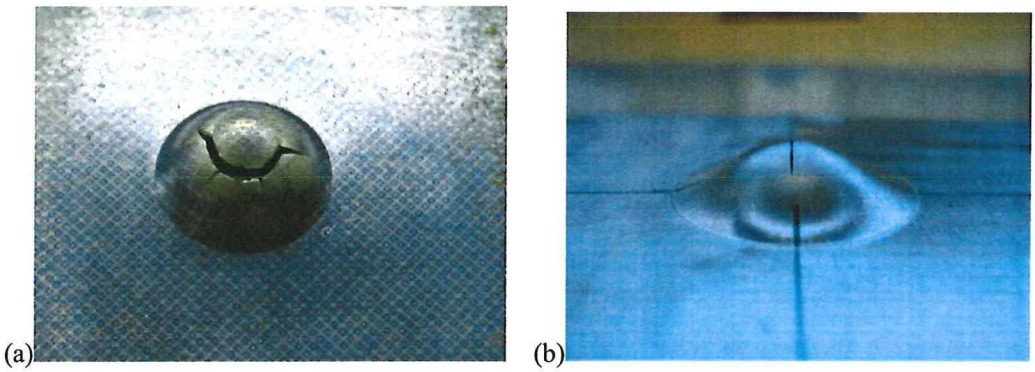

Figure 13: Failing of (a) a normal plate, the crack is circular (b) a bad weld, with a failure along the weld line

During Erichsen testing, the place of initial rupture can be observed as well as the deformation pattern. The speed at which the ball bearing was pushed into the weld was 0.161 mm/s.

Bending tests are sometimes performed to measure the formability, but not the most appropriate technique for the three-dimensional forming simulation of plates.

3.3.3 Hardness

Hardness can be measured after or during microstructural evaluation, the etchant only has a small influence on the hardness and will be neglected. The correct indent force should be chosen with respect to the microstructural evaluation (average hardness of weld material to determine material properties against the hardness of the phase to backup the phase identification). Hardness was measured with a computer controlled Vickers hardness tester and microscopic determination of the indent size and the related hardness was undertaken. The force chosen for a general evaluation was 300 grf and for the measurements of single phase areas it was 50 grf.
Standard procedures can be obtained from the standards (NEN, ASM, SAE; [46-48])

3.3.4 SEM

SEM specimens were prepared by polishing to 1 μm, a short etching (3 seconds) with 2% nital and were gold plated with physical vapour deposition to enhance the electrical conductivity of the surface. Local composition and definite structure recognition could be obtained from this evaluation.

3.3.5 Microstructural evaluation

Cross sections of the welds were made, mostly 1 cm from the side. These were mounted, ground and polished to 1 μm. To reveal structural features, Nital 5% etching [49, 50] for 8 seconds was applied as a standard procedure.
Several other etching procedures, like nital or picric acid etching with subsequent sodiummetabisulphite submersion [51, 52], LePera's reagent [53, 54] and Behara [55] etching have been attempted to improve contrast between ferrite, bainite, martensite and pearlite [1, 50]. These etchant can increase contrast between phases, but will not give conclusive information on the actual structure of the micro constituents. Also these etchants are sensitive for the storage time and can give varying results. Therefore these were regarded as too time consuming and abandoned.

4. Results and discussion

4.1 Results

An operating window should be obtained, with which the important process parameters define weld quality. This can consist of several small areas of parameter limits, which all give good welds, but probably only one area is present. At the moment the repeatability of the results for thinner plates is an uncontrolled factor, which has been optimised by the preparation of the butt ends. The quality of the weld is only measured in terms of mechanical properties and weld shape, but these are also explained from a microscopical perspective.
Other experiments were performed with the specific goal of measuring material properties. There are three features that have been studied: the influence of a heat cycle on the segregation, the austenitisation speed and the forging temperature.

4.1.1 Plain welding experiments

First the sequence of the programme were analysed to see when and how the transitions to the next steps were made. Then an evaluation of the mechanical, electrical and temperature measurements was performed to describe material handing during the welding process. Finally the specimen's microstructure and mechanical behaviour was analysed. A set back occurred because due to the forging action, the thermocouples broke off during welding and the data obtained could not be used for comparing different parameters combinations. The response time of the thermocouples was also longer than desired for the fast heating and therefore temperature measurements are not included in the study. Although the temperature is important especially for the determination of conditions under which the material was able to join and for the CCT determination of the final microstructures, an indicative measurement (Figure 14) has been performed at the middle of a sample, which gives general information on the heating and cooling rates for microstructural analysis with CCT diagrams. The heating and cooling rates that have been observed were respectively 750 °C/s and 150 °C/s.

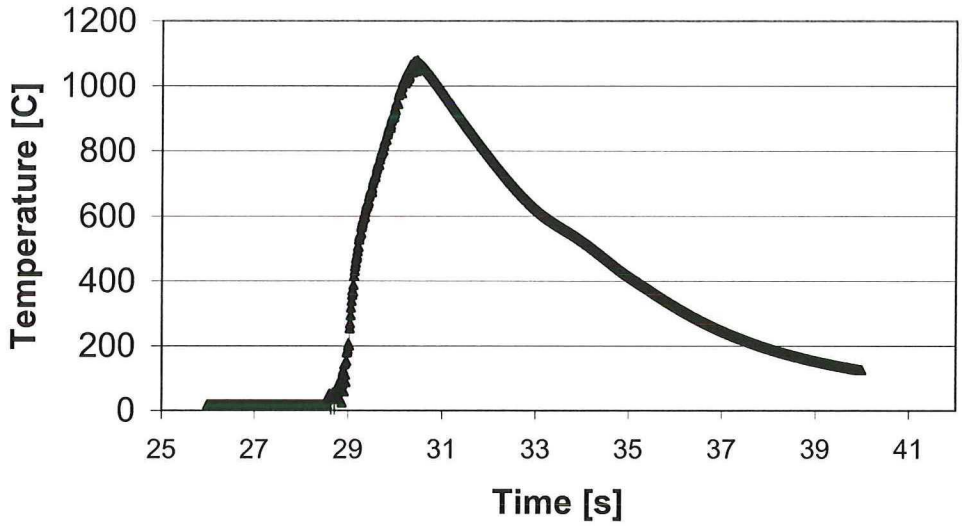

Figure 14: Temperature cycle in the middle of a weld seam

4.1.1.1 Weld programme sequence

The transition of two undetermined steps of the programme can now be specified according to the experiments. In the experimental procedure it was already indicated that the first, fourth and fifth steps had a fixed transition condition.

Taking the program of Table 2 as an example of a weld program, in Table 4 the conditions for the change are indicated by the bold numbers. It has been observed that at low current densities (<90 A/mm^2), the material was not softened enough to complete the second step of heating. In those conditions the upset was sometimes forced after 2000 ms of heating and the material was too hard to accomplish the upset distance in the total time available for the whole process (3000 ms). This means that at low current densities the apparatus can only continue delivering heat to soften the upset material during the total maximum time for the upset step (a second). When this is not long enough to attain the full upset distance, the upset movement will be stopped and the rest of the program is aborted.

Table 4: Analysis of the weld program

P [MPa]	J [A/mm2]	dx [mm]	dt [ms]
70	0	1.0	**100**

Table 4 (continued)

80	100	**0.3 (≥90A/mm²)**	**2000 (<90A/mm²)**
100	100	**5.0 (≥90A/mm²)**	2000
40	0	1.0	**100**
10	0	1.0	**10**

The peak temperature will influence the amount of upset created at the applied pressure. At low current density (80 A/mm^2), the heating is not sufficient and the upset will be forced to start by the time restriction. The acceleration at the end of the second step by the increase of the pressure is visible in all of the low current measurements at 2.1 seconds (Figure 15). As can be seen the initial speed of deformation directly after the increase of the pressure varied, which indicates that the softening started, but an upset distance of 5 mm could not be achieved and only in one of the 80 A/mm^2 samples the 3 mm upset distance was obtained. This lack of completion means an insufficient forging action, with too little interface movement to redistribute the surface contaminants along the weld and partially into the (limited) upset (Figure 16).

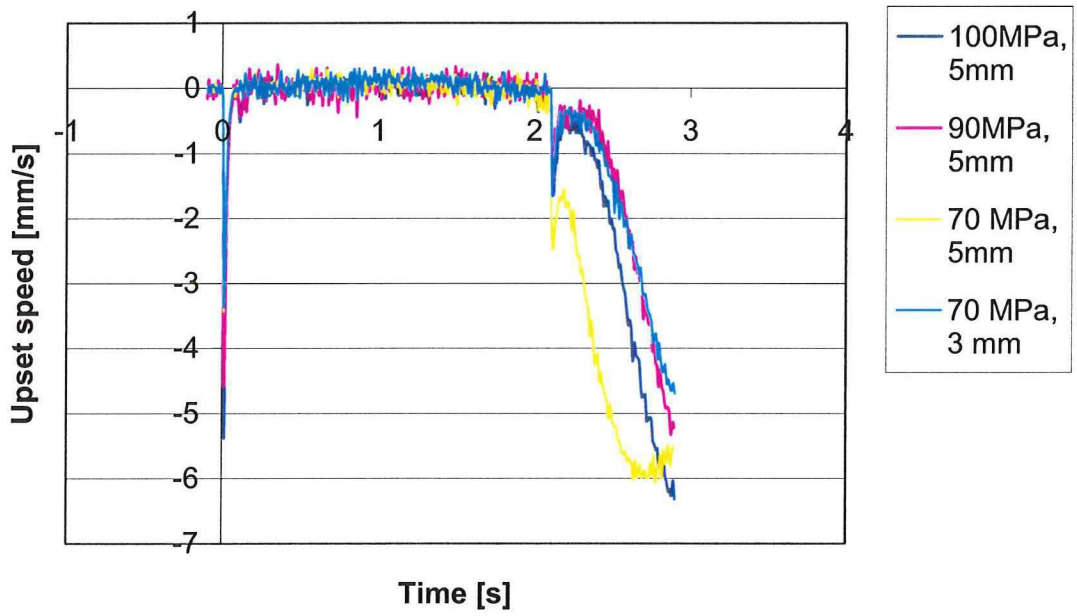

Figure 15: Upset speed in a low heat input (80 A/mm^2)

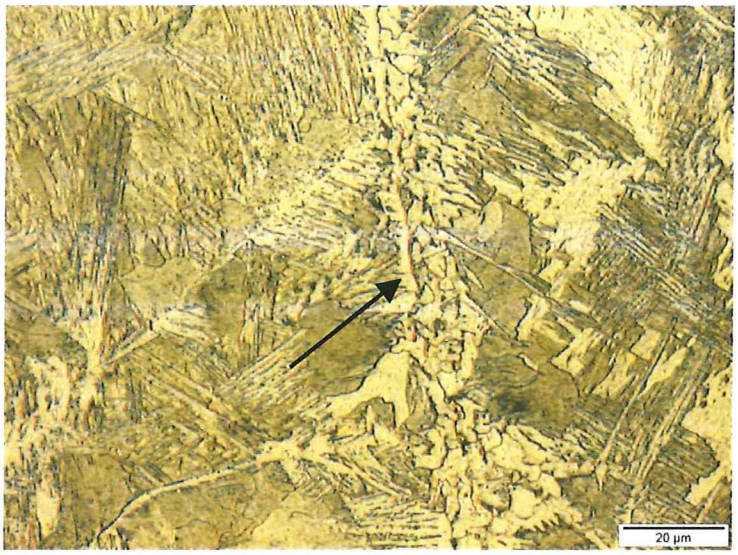

Figure 16: The bond line still visible in a specimen welded at 80 A/mm^2 and 70 MPa

In specimens with higher current density ($\geq$ 90 A/mm^2), specimens were hot enough to soften and start the upset stage by the deformation condition. The effect of softening is especially visible in the pressure drop (arrow in Figure 17) just before the upset pressure is applied.
In all specimens with a current density of 90 A/mm^2 and higher the requested upset distance was achieved. The rate of deformation differed, indicating that the extension of the softening varied, but this will be discussed in the section on mechanical treatment (4.1.2).

4.1.1.2 Mechanical, electrical and thermal treatment

This section is an overview of the weld conditions and, after welding and analysis of the microstructure, an objective judgement can be made concerning the weld quality. Although this is descriptive, some welds that have experienced an incomplete welding cycle can already be classified as having insufficient quality.

The start of the upset at higher current densities is determined by the softening (indicated by the arrow in Figure 17), and thus the heat input. It has been observed that at low axial pressure, the initial heat input after half a second can vary extensively (Figure 18). At higher temperatures the initial variation of the contact resistance diminishes and the heat input per second will be equal.

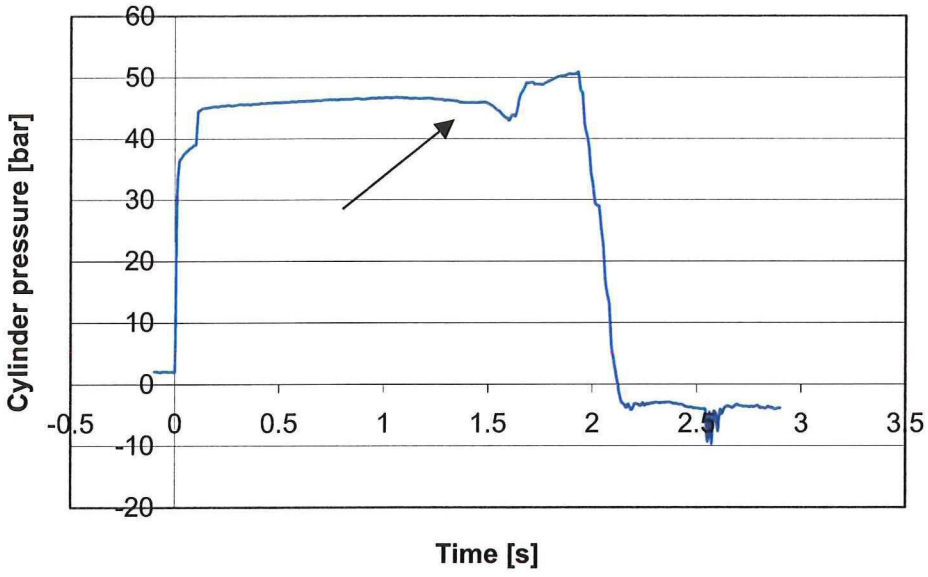

Figure 17: Average upset pressure of three samples welded at 100 MPa, 100 A/mm^2 and 5 mm upset samples

This means that there can be a slight shift in the start of the upset for varying starting conditions, but at an equal parameter set-up. The moment of deformation is globally the same at varying pressures. At high pressure the bulk resistance remains the same and since the contact resistance is smaller, less heat will be conducted to the peripheral zone, which will be at a lower temperature than at low pressure. Since only three different pressures have been employed this effect can change at lower or higher pressures. At very low pressures, the contact resistance might vary in another manner than at the employed pressures as it is more dependent on the interface properties, while at very high pressures it will become harder to decrease the contact resistance as there will be more material on the surface that has to be flattened.

At low current density (80 A/mm^2) the material was softened enough to deform the material plastically at the relative low pressure level ($\sigma<\sigma_y$; σ = 70-100MPa compared to σ_y = 370 MPa at room temperature) but the speed remained low (100 MPa, 80 A/mm^2 in Figure 19). The material is forgeable but has not yet softened and therefore the requested upset is not obtained. At 90 A/mm^2 the material became forgeable within the heating time limit and the heating was extensive enough to continue heating of the weld metal along the upset direction throughout the upset process (100 MPa, 90 A/mm^2 in Figure 19). When at the beginning of the upset the material is hot enough to obtain an extensive upset distance *(>2.5 mm)* in one movement, upset speeds of up to 30 mm/s were recorded. At this point (J $\geq$ 100 A/mm^2) the material is not only forgeable, but also softened.

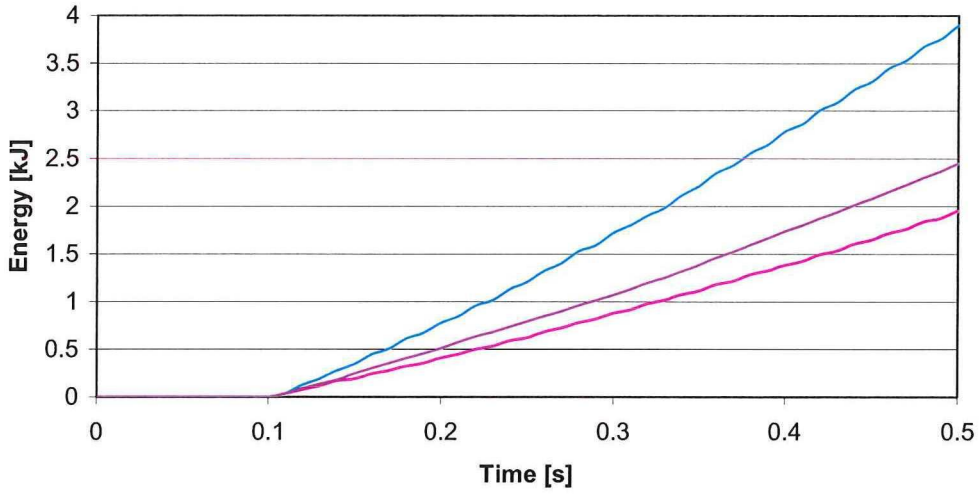

Figure 18: Energy input calculated by the delivered Joule power for three specimens welded at 70 MPa, 100 A/mm^2 and 5 mm upset distance. Differences may be due to contact resistance phenomena or variations in welding machine performance.

During the upset, colder material is sometimes pushed into the weld seam and slows the process when the metal that is forgeable but not softened is being deformed. Depending on the deformation that can be obtained in the single movement, upsetting continues in the forging regime (70 MPa, 90 A/mm^2 in Figure 19), or the complete upset can be reached within 0.2 seconds creating a smooth deformation chart when it is totally softened (70 MPa, 100 A/mm^2 in Figure 19).

At intermediate heat input (90A/mm^2), it can be seen that initially upset was performed smoothly, but when the cold material was pushed into the weld zone, upset speed decreased and deforming demanded more effort. Above 100 A/mm^2, speed profiles look smooth, but a decrease in speed remained, indicating that the machine starts to struggle to move the colder upset material into the weld zone. At high pressure the softened to forging transition is more distinct than at low pressure. Whether this originated from lack of data in between or that at high pressures, the speed obtained will be maintained due to machine inertia, is unknown. In the samples with 3 mm upset the end of the upset is reached within the soft range and a sudden stop is executed after obtaining the total upset.

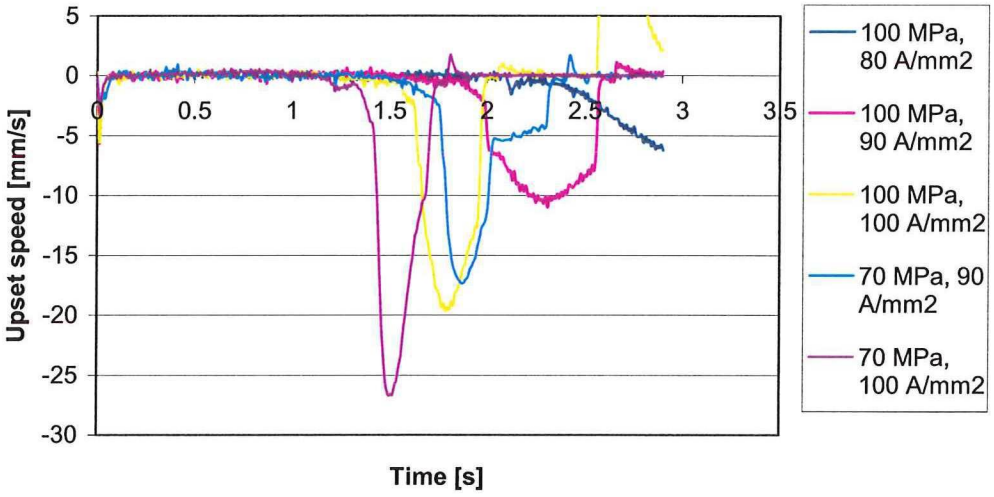

Figure 19: Varying deformation patterns at different weld setup, all specimens welded along 5 mm upset distance

During welding localised heating was observed a centimetre from both edges of the weld seam; these spots had a higher heat input and reached a higher temperature than the middle of the weld seam.

The role of the uneven heating in the process of deformation is not quite clear. As the sides heat faster, contact resistance will probably diminish on those places, mainly as a result of the high temperatures, but resistance will increase according to the increased resistivity at higher temperatures. The middle of the weld seam will then have a relatively low resistance (even with

the contact resistance included), but the heat development is still lower than at the sides. So heat will be created more evenly but not according to a completely flat profile. When the middle has softened, the upset movement starts and is generally uniform along the weld seam. Because of the higher temperatures at the side, a different deformation pattern will be created, which is the result of intergranular melting in high solute regions and the extreme softening at these places.

Upset formation differs between extensive softened material and that which is normally softened or only forgeable. The hot spot material is so soft that it is expelled from the weld and does not form a real upset, but a plume-shaped upset with a narrow stem (Figure 20a). Colder metal will be forged together and create an upset which can be characterised as bead shaped (Figure 20b). The larger upset size at the lower side is constant but originates from the misalignment and not gravity, because the material is considered still strong enough to bear its own weight.

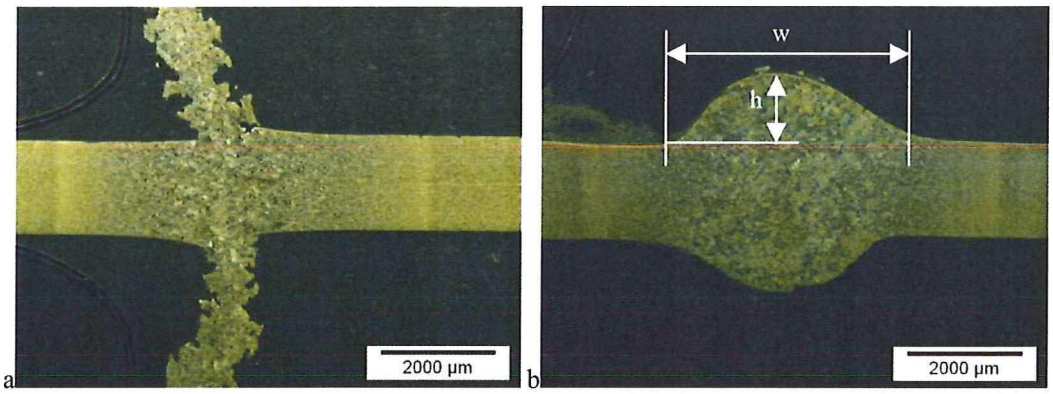

Figure 20: Upset shape in a) a hot spot with plume shaped upset and b) forged upset with bead shape (pictures are upside down compared to the weld setup). In both pictures the misalignment can be observed.

Whole plate comparison

Joule heating was slower due to the lower resistance, but eventually potential differences became equal (Figure 21), indicating that a fully electrical contact has been established in the welds. Increase of the resistance at the end of the upset movement can be fully attributed to the increased temperature dependent resistivity.

The obtained microstructure is similar to the welded samples, and the mechanical properties were only slightly altered; Erichsen height was 1 mm less than that of the base plate indentation (11.6 mm). This indicates that the microstructure after welding is not the critical feature, but the

process of welding itself is not sufficient to create perfect interface coalescence and the material will already crack along the weld line at low deformations.

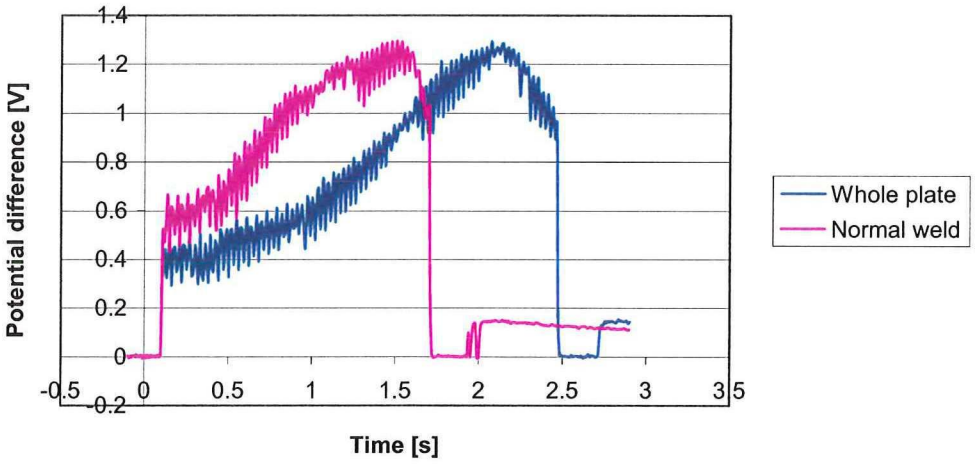

Figure 21: Slower increase of potential differences and heating when contact resistance is omitted

Repeatability

Repetition of experiments was sometimes difficult, because the interface properties were not constant. Initial heating depends on these features, and small differences can have big consequences. Idealising surfaces for example by milling the surfaces can be done in scientific experiments, but will be harder to implement in a production environment.

Higher pressure during heating does seem to decrease the variation in heat input, but the welds made at higher pressures did not perform well in formability tests until now (see section on formability and hardness). Increasing current density will only extend the initial differences, but a slow upslope can first decrease the interface resistance, giving the material the chance to close the opening gap that is formed by the surface irregularities. The idea is that the initial current will hardly contribute to the overall heating of the material. When the current is then increased the resistance should be equal for all samples.

Heating was unevenly distributed along the plate width. At the sides of the interface, heating was quick, but the middle lagged behind and seemed to warm mainly by heat conduction from the hot sides to the middle. The increased current density at the edges of the weld seam was also visible

during the application of the weld program to a whole plate, meaning that the hot spots arise as a result of the current application and not interface related features.

Three possible electromagnetic effects are generally associated with converging of the current: the right hand rule, the skin effect and eddy currents. The first is a DC effect where the currents are pulled to the surface by the Lorentzforce according to figure 22. AC waveforms can cause the skin effect, but an alternating sign of the current is required [56]. Since the current is not constant but oscillating (figure 23) the current can be disturbed by the varying magnetic field and cause turbulences in the current [57]. These vortexes are called eddy currents and are often applied in high frequency applications such as microwaves. In the welding, it is not clear how these turbulences develop. Further research with attention to the influence of Lorentzforce and eddy currents on hot spot formation will be executed.

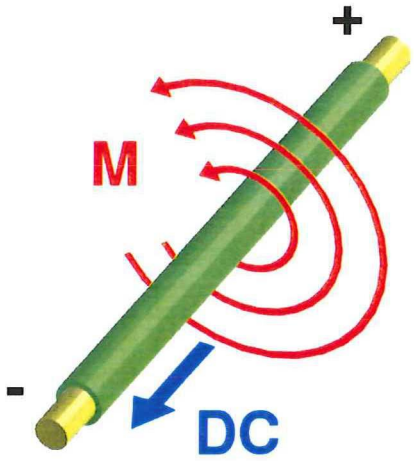

Figure 22: The creation of a magnetic field around a unidirectional DC

At the beginning of the upset, due to the increased pressure, the interfaces begin to make contact throughout the weld interface. As the middle experiences less heating its resistance is low and the overall potential difference drops as the contact resistance diminishes. After this drop, heating is continued and resistance will rise again due to the increasing resistivity.

It was perceived that in the hot spots during the upset, plates partially do not form a bead but plume shaped upset; by the high heat and thus softening the angle at which the displaced material moved was perpendicular to the plate. One side of the upset shows a clean surface (arrow in Figure 24) that has been broken up. On the other side melting or the high pressure movement

disrupted the material (Figure 24b). When this shoving occurred on both sides of the weld seam (front and back), one plate always crawls underneath the other, indicating that the alignment was not perfect (Figure 25).

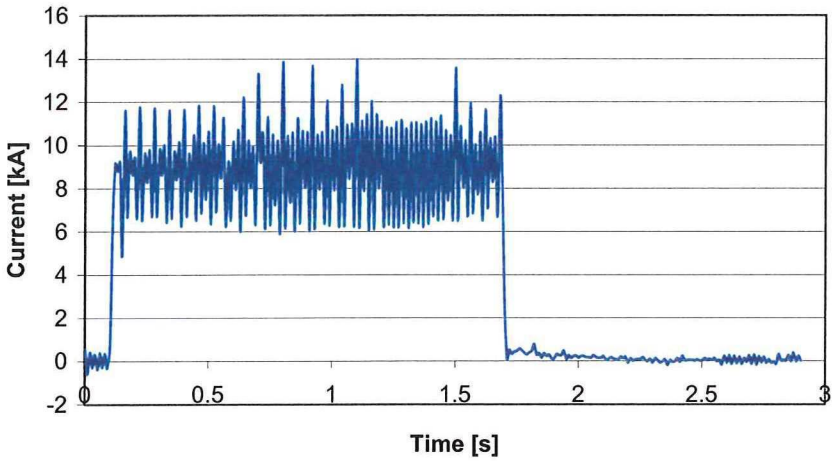

Figure 23: The measured current in a 70 MPa, 100 A/mm^2 and 5 mm upset distance specimen

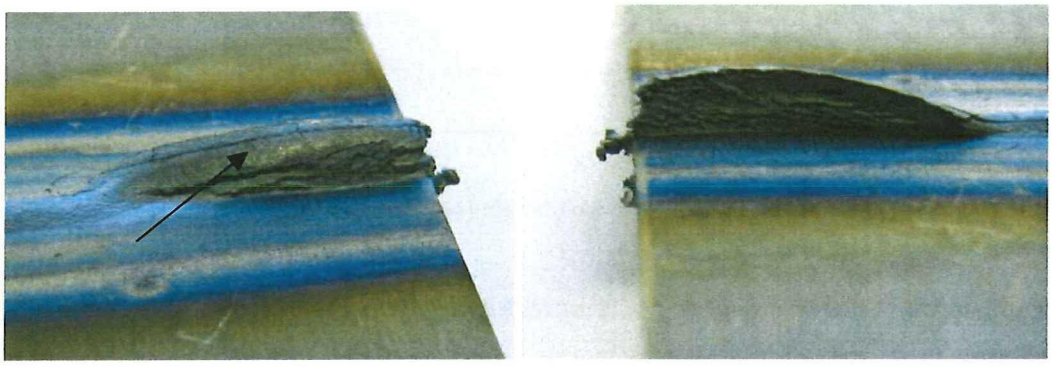

a b

Figure 24: a) the smooth but broken surface and b) the disrupted surface

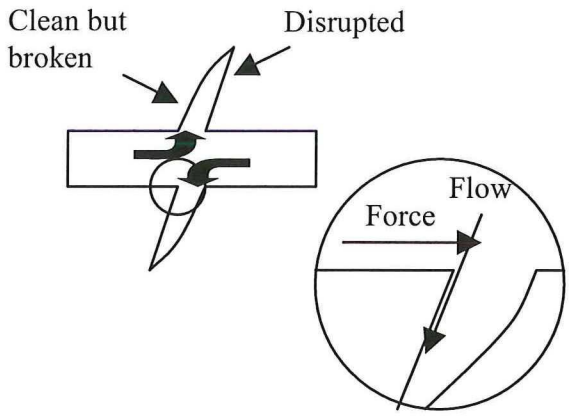

Figure 25: Schematic drawing of the material flow in hot spots, black arrows indicating the material flow, in the overlay it can be seen that the material is disrupted at the place where the force and flow cross

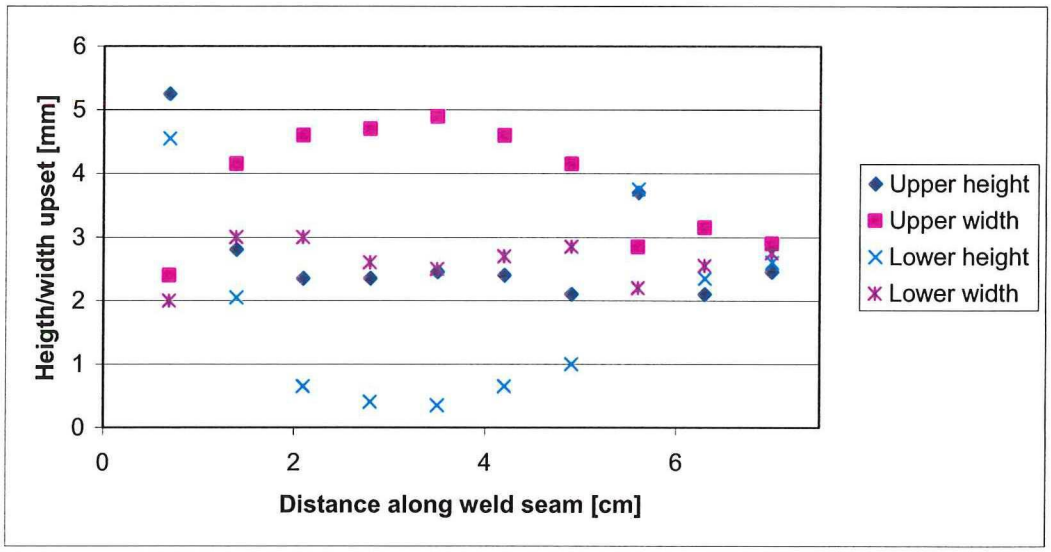

Figure 26: Upset dimensions of a specimen welded at 70 MPa, 100 A/mm^2 and 5 mm upset distance

Measurements on the weld dimensions were performed according to the scheme shown in Figure 20b. The base of the height was the side that was the greatest distance away from the top of the upset, which was the right plate in the machine setup.

The small width of the upset (~ 2 mm at hot spots in comparison to 4.5 mm in the middle, measured on the lower side of the weld) is a result of the very high softening, thereby not creating

stresses in the peripheral zone of the upset. Parts with lower temperatures induced stresses along a longer length perpendicular to the weld seam, causing it to deform.

Another option is that the material has a high temperature brittle area, when impurities are concentrated and dragged along the austenite grain boundaries while the austenite growths. These impurities can lower the melting temperature and the grain boundaries can melt at lower temperatures. The material can then fail without any preceding deformation. Broken areas on the grain boundaries should then be visible on a micrograph or with ultrasonic evaluation. The length of the cracks will be in the order of magnitude of the austenite grain diameter (~100-200 µm). This theory is supported by the angled cracks that appear next to the centre of the weld (Figure 27). The greater gaps (black areas) are cracks that have been torn open by the upset movement. The slightly lighter structure at the right hand side is the weld metal. With SEM analysis it is shown that the angled parts of the crack exhibit melting (Figure 28a) and that further along the crack the signs of melting have diminished and the crack has been torn open mechanically (Figure 28b). The small cracks, which are visible in Figure 27 are considered to be the result of melting, but are not cleaved during upset.

Iron or manganese sulphide precipitates that are associated with intergranular melting [40], has not definitively been observed with optical microscopy .

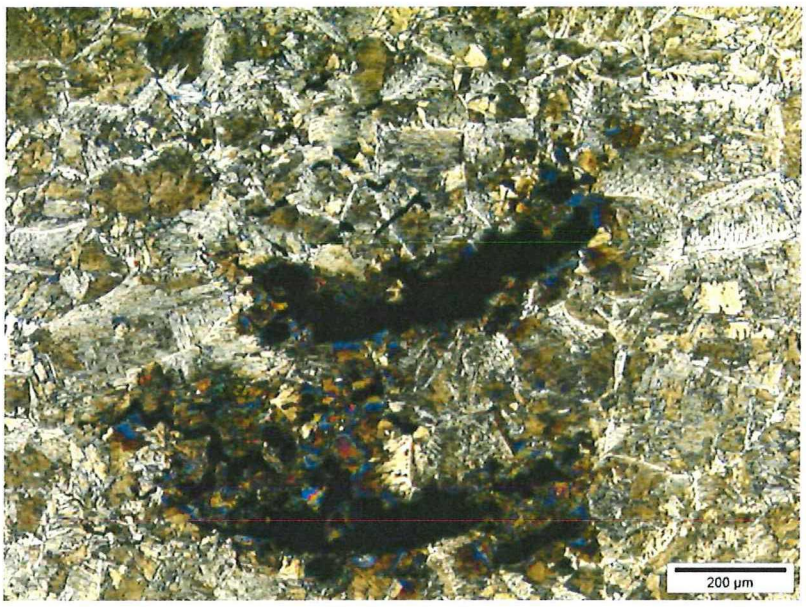

Figure 27: Crack formation in the peripheral zone of the weld

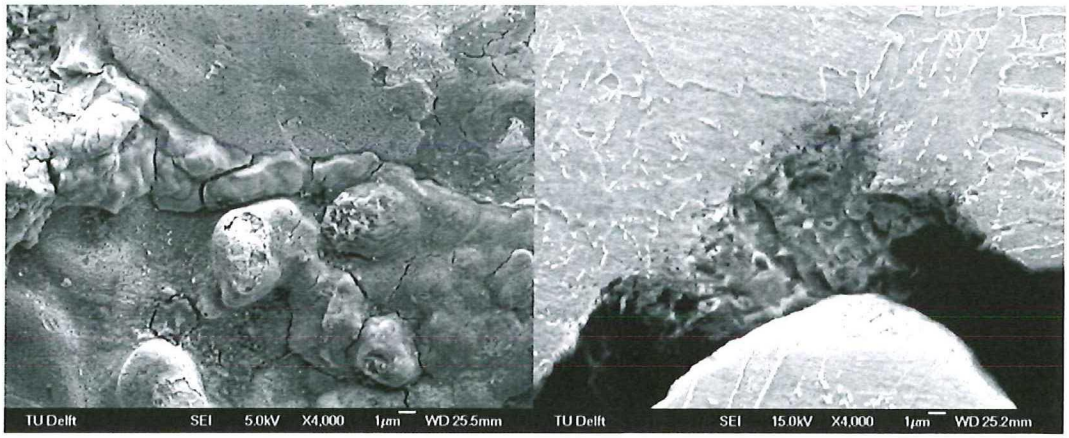

a b

Figure 28: SEM recording of the inside of the upper crack in Figure 27

Alignment

During experiments it was noticed that the plates are not always aligned. This promotes a certain flow pattern during deformation, where one plate can slip underneath the other. Crevices can be formed at the weld seam especially the topside as the upset movement pushes the soft material downwards. Whether this can be eliminated by a normal forging action without hot spots is unknown. The misalignment is present but the effect is not yet as critical as the hot spot formation.

The misalignment is a small (2-3°) angle between the plates in the plane that is perpendicular to the weld seam (misalignment mode of Figure 4c).

Formability and hardness

Due to the formation of a ferrite-pearlite structure, the welds are not significantly harder than the base metal. Due to the small free path for dislocations, the structures are generally considered to resist smaller deformation than an allotriomorphic ferrite structure, even with dispersed bainite. Initial grain size in the base metal is small, creating a comparable path length, but the carbides between Widmannstätten fingers are more efficient in blocking the dislocation motion.

As is shown in Table 5 the deformations obtained in the specimen were lower than expected for the weld metal, only at high current where the material was softened was good formability found. Cracks were mainly found along the weld seam, indicating lack of bonding. As the samples were

tested in the middle of the material at the point of lowest heat development, it is possible that the forging action was not sufficient to remove interface contaminants and obtain a good joint.

Table 5: Erichsen measurements

	h [mm]	F [kN]	
Base sheet properties	11.72	31.9	
Upset pressure 100 MPa			
80 A/mm^2	3.37	5.3	Forged
90 A/mm^2	3.23	3.1	Forged
100 A/mm^2	3.23	3.2	Softened
110 A/mm^2	2.87	3.0	Softened
Upset pressure 90 MPa			
80 A/mm^2	3.30	4.0	Forged
90 A/mm^2	3.63	4.0	Forged
100 A/mm^2	3.18	3.1	Softened
110 A/mm^2	3.18	4.0	Softened
Upset pressure 70 MPa, 5 mm upset distance			
80 A/mm^2	3.00	3.4	Forged
90 A/mm^2	3.06	15.1	Forged + Softened
100 A/mm^2	7.24	14.9	Softened
110 A/mm^2	4.48	7.4	Softened
Upset pressure 70 MPa, 3 mm upset distance			
80 A/mm^2	3.45	5.0	Forged
90 A/mm^2	4.07	5.7	Forged
100 A/mm^2	4.60	8.7	Softened
110 A/mm^2	6.68	21.9	Softened

The hardness measurements of the weld show that the weld is significantly harder than the base material (200 compared to 170 HV0.3, repectively), but is much less distinct than hardness differences in other welding processes (~ 100 HV per 2 mm, [49]). The low carbon content ensures a structure that when cooled in air will not be hardened extensively.

4.1.1.3 Microstructure

Optical microscopy

In all welded specimens the structure that was found consisted of ferrite and a second (from the etching procedure) brown phase that could not be identified definitively with optical microscopy (Figure 29). This difficulty has two causes: first the dispersion of carbides is too fine and light microscopy cannot resolve these. Secondly nomenclature in ferrite and second phase constituents from the literature can be confusing and several authors have made their own classification [58-60]. Industry often still uses the older categorisation with terms such as sorbite, troostite and others, which were found ineffective for the new grades of steel and the new insights in metallurgy based on kinetic and thermodynamic knowledge of phase transformations. In the present classification ferrite is subdivided into allotriomorphic, idiomorphic and Widmannstätten ferrite. Second phase types are pearlite, bainite and martensite (with possible residual austenite), of which pearlite and bainite have subdivisions. Acicular ferrite is not directly placed in any of these categories, but often all intragranular nucleated plates or laths are associated with acicular ferrite.

In the weld samples ferrite has grown through different mechanisms, leading to several morphologies. Widmanstätten ferrite was the dominating morphology, but allotriomorphic ferrite on the prior austenite grain boundaries was also observed. The ratio of these types of ferrite varied with peak temperature and cooling rate in different places in the weld.

In SEM analysis no lamellar structure was observed in the weld metal, but only dispersed carbides were seen along the same orientation. Hardness measurements on a single phase area were performed and resulted in a hardness of 200 HV_{50g}, which categorised the brown phase as pearlite. Together with the fine carbide dispersion, the phase was identified as non-lamellar pearlite. This structure has also been named granular bainite [59], but the growth mechanism of the two phases determines the difference and exact morphology.

Although the structures along the weld seam are similar (Figure 29), there are differences in the amount and size of each phase. At the sides, the pearlitic structure is less dominant due to a faster cooling rate than in the hot spot. 1.4 cm from the side almost all ferrite grew in a lath structure where in the hot spots and at the side, grain boundary ferrite has grown. The amount of pearlite is less then in the hot spot. In Table 6 a rough visual estimation of the amount and type of ferrite along the weld seam can be found.

In the hot spots the bond line appeared lighter after etching (Figure 30), it is unclear whether melting, carbon depletion or a cooling rate where only lighter etched structures developed causes this feature.

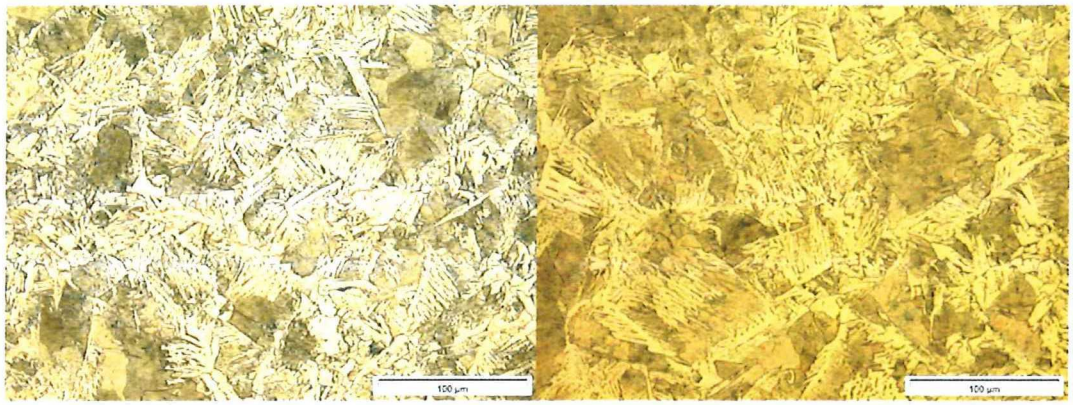

a b

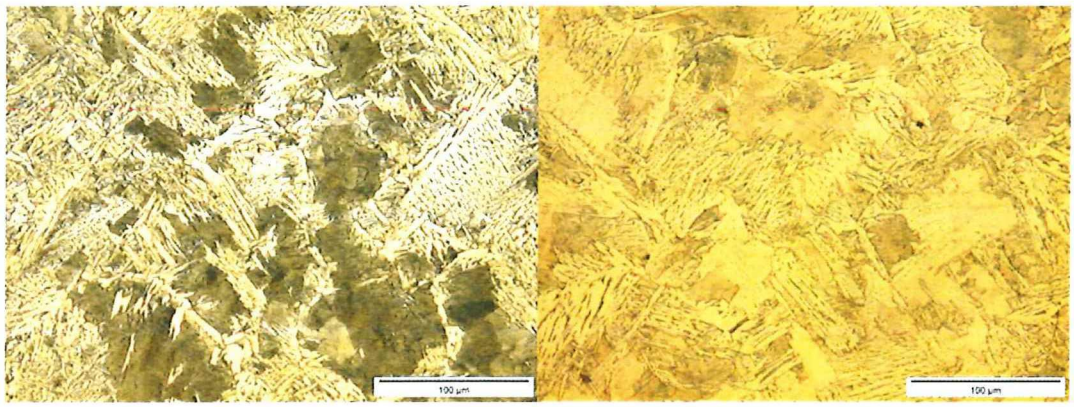

c d

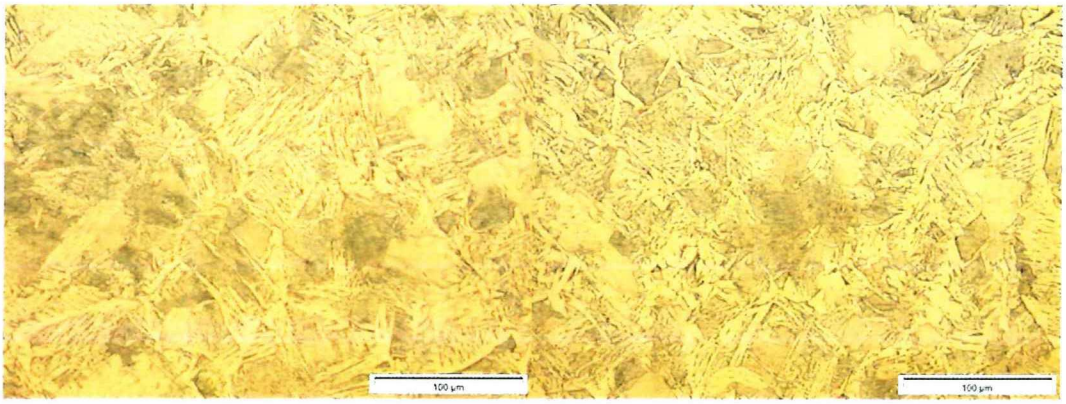

e f

Figure 29: Weld structures along the weld seam from the surface with steps of 7 mm (a) being the surface and (f) the middle of the weld

Table 6: Amount and type of microstructures along the weld seam

Place (index in Figure 29)	Estimated amount of ferrite (%)	Morphology ferrite
0 mm (a, the side)	70	Lath and grain boundary
7 mm (b)	60	Lath and grain boundary
14 mm (c)	75	Lath
21 mm (d)	80	Lath
28 mm (e)	70	Lath
35 mm (f, middle weld seam)	80	Lath and grain boundary

SEM

In the SEM analysis, black spots with bright surroundings have been reported (Figure 32). This look is typical for holes, the white refection is a result of the edge effect. Electrons are more easily emitted from edges, because the material energy function promotes these places for electron emission. These are most likely pieces of material ripped out during sanding or polishing. The structure of the second phase of the base material was observed (Figure 31) as well as the structure that formed after welding (Figure 32). Finally the nature of the cracks that formed in the hot spots was further analysed.

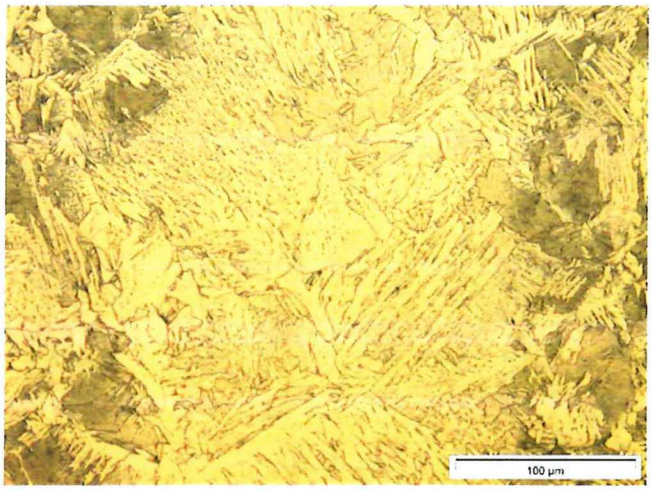

Figure 30: Lighter appearance at the bond line in the hot spot

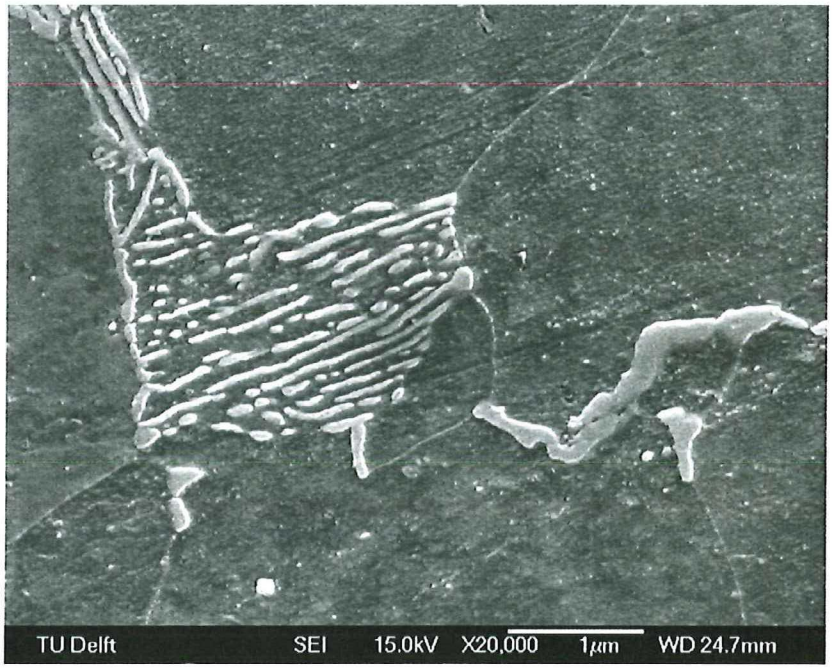

Figure 31: Base structure of HR 45

Figure 31 shows an example of the second phase morphology. The growth of the cementite is not throughout the whole particle, but looks slightly spherodised. Upper bainite in this structure does not have the feathery look with which it is often associated [61].This can be explained by the growth in the residual austenite while ferrite has already been formed it is limited to the small

areas and does not grow into a large austenite grain. The strong orientation with respect to the former austenite implies that the second phase morphology is indeed bainite. Pearlite has a more random orientation that originates from the diffusional growth system.

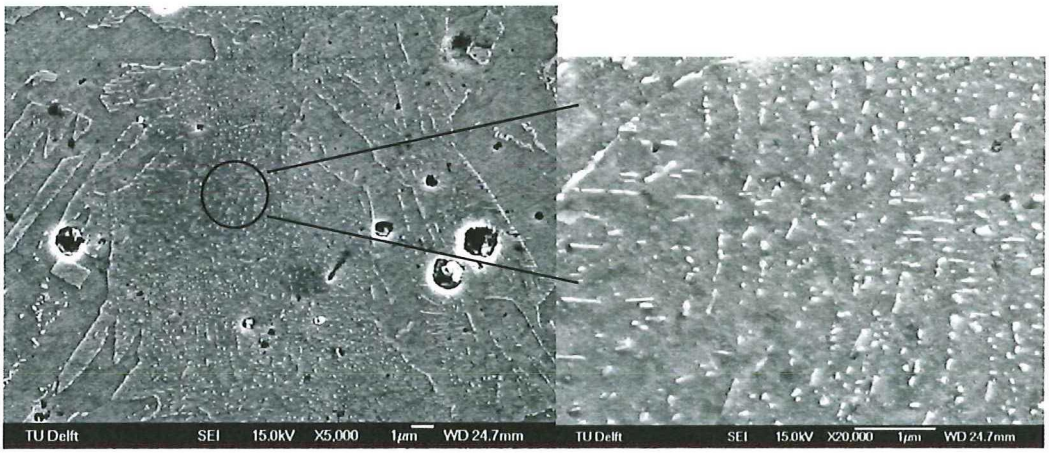

Figure 32: SEM recording of the weld metal, showing non-lamellar pearlite and in the lower left corner Widmanstätten ferrite

The weld structure contains small carbides (overlay in Figure 32), which share a common orientation. Carbon enrichment in the remaining austenite has not been so extensive that fully lamellar structures could develop. The orientation is not comparable to that of lower bainite as the carbides should also have a fixed orientation with respect to the ferrite laths. Since the measured hardness of the phase was 200 $HV_{0.3}$ the structure is formed in a pearlitic growth system but is underdeveloped. Both reasonings lead to the conclusion that the second phase is a non-lamellar pearlite. Widmanstätten ferrite could already be seen in optical microscopy with small second phase particles between the fingers.

The optimisation of the contrast between different types of second phase is difficult. Reaction of bainite and fine pearlite structures to the etching procedure is similar. Although the final microstructure has already been mentioned and seemed fairly straightforward, the determination had more to it than just observing the structure through microscopy. As the material is a ferrite matrix with relative hard second phase, hardness measurements will not resolve the very small second phase particles. The hard particles can be pushed into the matrix, measuring matrix hardness and not the second phase.

Etching would supply enough contrast when the right etchant is chosen. Although there are some chemicals that should be able to give bainite another colour than pearlite, these procedures can be sensitive to the time between the making of the etching solution and the etching, small pollutions on the surface and whether the specimen is mounted or not. After trying different etching procedures, the best contrast was found with picric etching with subsequent 10% sodiummetabisulfide. This contrast was especially between the ferrite and the second phase, but did not reveal the nature of the second phase microstructure in neither base or weld material.

After SEM analysis it was believed that the lath or plate like morphology in the base metal was indeed bainite as specified, but in another research a similar structure was determined as pearlite [62]. More literature research showed that the range of carbide thicknesses in pearlite did envelope that of bainite spacings and could even be finer. The carbides that have been observed in the SEM analysis do seem large in comparison to the ferrite and are overdeveloped for bainitic cementite. Carbides are less attacked by the etching agent and will be a little above the surface, therefore they will be enhancing the electron emission, thus the thicker look of the carbides can be misleading. Conclusive information should follow from further TEM analysis of the supposed bainitic ferrite, which should show the effects of a displacive transformation and only small interlath and maybe intralath carbides.

Another aspect of the studied literature was that pearlite is not always found as a lamellar structure. The carbides look more spherodised, this effect can be caused by two process conditions: too fast cooling or too slow cooling. In the first event, the carbides did not receive enough carbon through diffusion, while the growth system is still diffusive, to cause lamellar formed carbides. This feature seems similar to the formation of lower bainite, but is thus underdeveloped pearlite. The content of carbon in the pearlitic ferrite might be increased, since not all carbon could have diffused to the cementite. After cooling that has been slow, the lamellae can have been spherodised, but these carbides should be larger since they are the product of relative long time at pearlite forming temperatures.

4.1.2 Specific experiments

4.1.2.1 Segregation homogenisation

The temperature control during the experiments was sufficient and during cooling the released austenite to ferrite/pearlite phase transformation energy could be observed as a decrease in the cooling rate (black arrow in Figure 33).

Figure 33: Temperature profile of a segregation sample

No dissolving of the segregation band has been observed with optical microscopy. A segregation band can be observed both in the base material and the heat-treated samples, but quantification without applying more advanced techniques was not possible. This means that the assumption that the segregation could be analysed with optical microscopy was premature. Etching is not so sensitive to the composition as hoped and secondly the quantification cannot be objective with this method, because the width of the band will be judged subjectively. A manner to improve this experiment will be discussed in section 4.2.

So-called ghost lines have been observed during these experiments (Figure 34). These lines are visible in micrographs of both the base and heat-treated metal, but do not *per se* have corresponding features in the microstructure. The lines are orientated in the rolling direction and therefore two logical origins can be mechanical stresses or the segregation. The latter has been investigated by Stewart *et al.* [63] and associated with the phosphorus content differences.

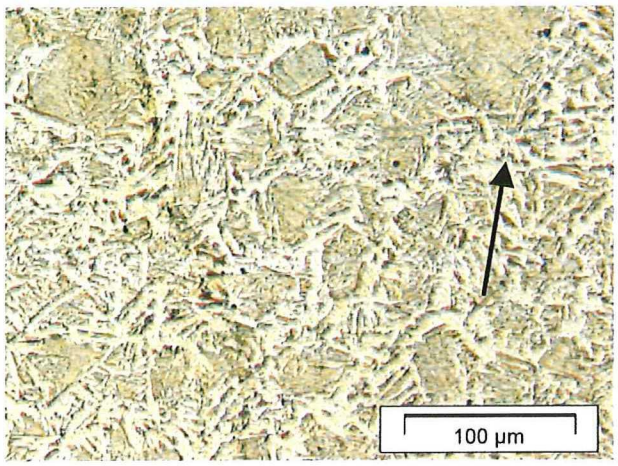

Figure 34: Ghostlines in the heated sample

A second observation was that in a 1 second heating and 1 second holding time and water quenched specimen the structure was completely martensitic (with some retained austenite) and therefore must have been transformed completely to austenite in this time (Figure 35).

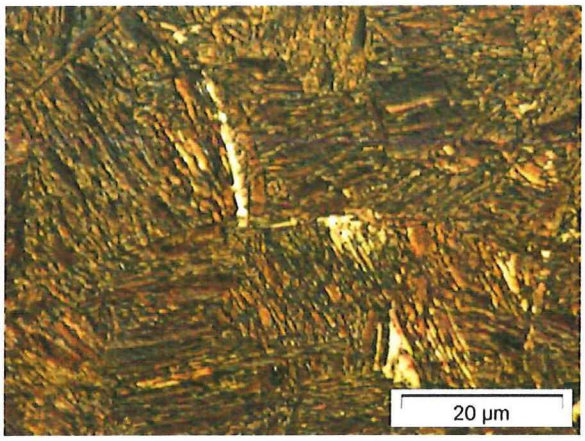

Figure 35: A fully martensitic structure after 1 second heating to 1100 °C and a holding time of 1 second

4.1.2.2 Austenitisation speed

From these experiments two ways of determining the transformation temperature could be extracted. The Gleeble can be employed as a rough dilatometer and from micrographs it should be visible whether the ferrite or bainite has transformed to austenite and vice versa.

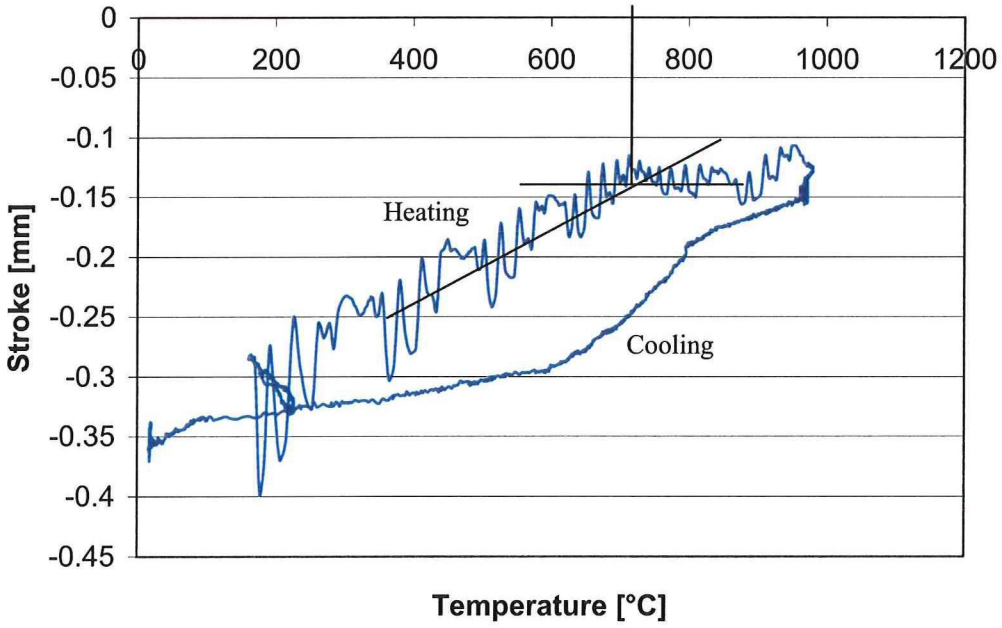

Figure 36: Displacement as function of temperature

During heating the current was applied in pulses, which can also be recognised in the varying stroke (absolute position of the clamp) in Figure 36 and therefore the transformation temperature to austenite cannot be seen clearly. Although the thermal expansion coefficient does seem to change at around 700 °C in this graph, the austenite-ferrite transition temperature cannot be determined from the oscillating stroke. During cooling the stroke is smoother and the transformation temperature should emerge more clearly. But since the objective was to measure the base structure to austenite phase transformation, the temperature determined during cooling will not be representative because of the temperature shifts that are present due to superheating and undercooling.

A clear transformation trajectory could not be determined microscopically as a result of the broad step width (Figure 37). Still a transition starting and finishing point can roughly be determined. Up to 800 °C hardly any austenite is formed, but the bainite tempers and the carbon diffuses to the grain boundaries and forms a feather like structure. Between 800 and 900 °C austenite begins to transform and is fully transformed at 1000 °C. It is notable that a faster transition is seen at a heating rate of 400 °C/s, but is fully understandable considering the shorter time for transformation at a rate of 800 °C/s.

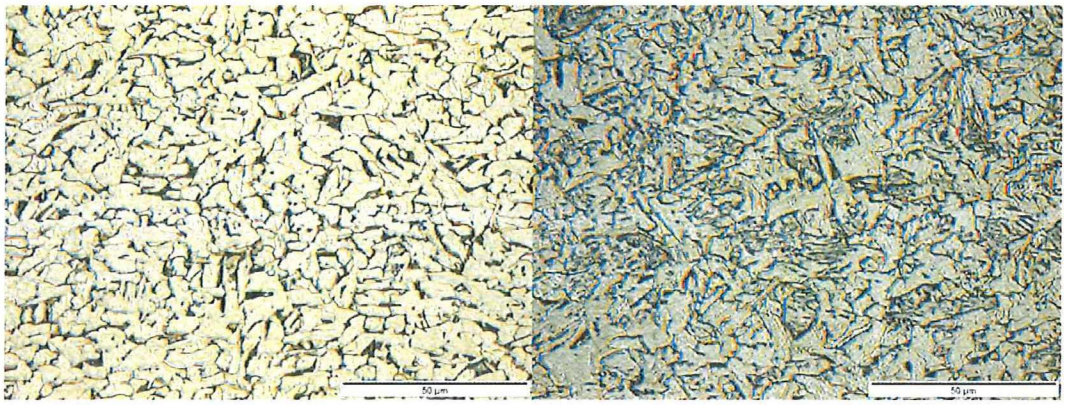

a b

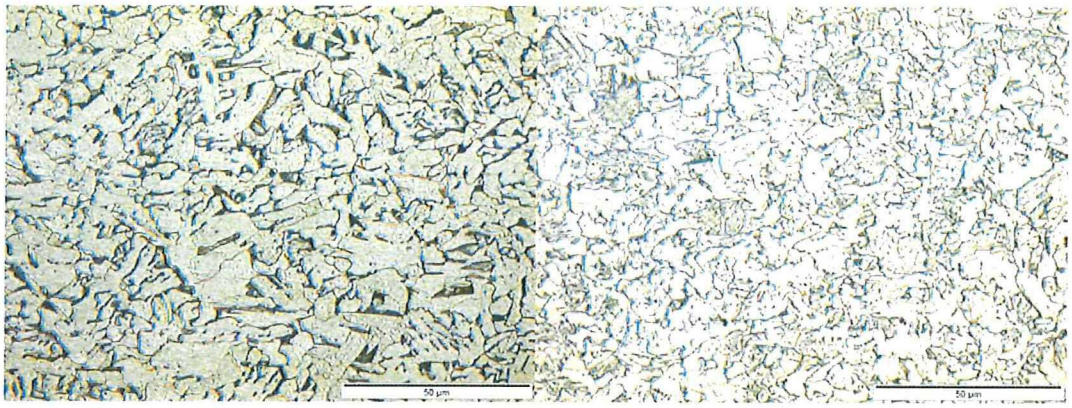

c d

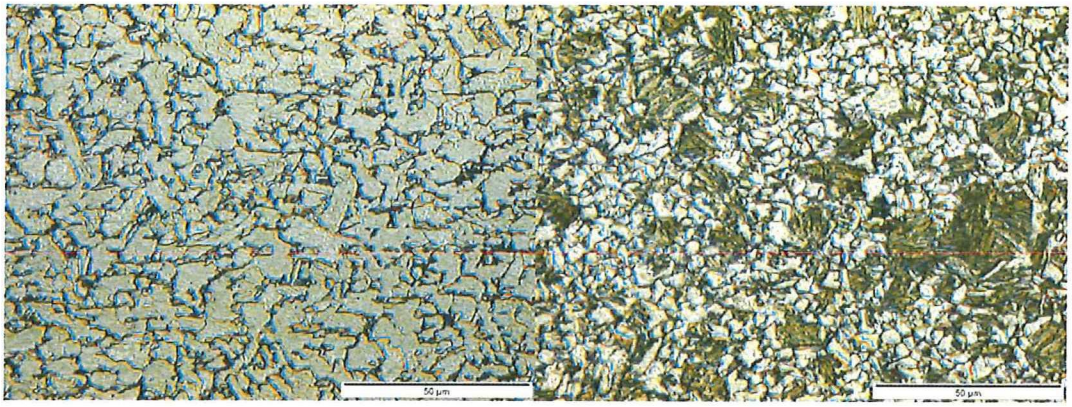

e f

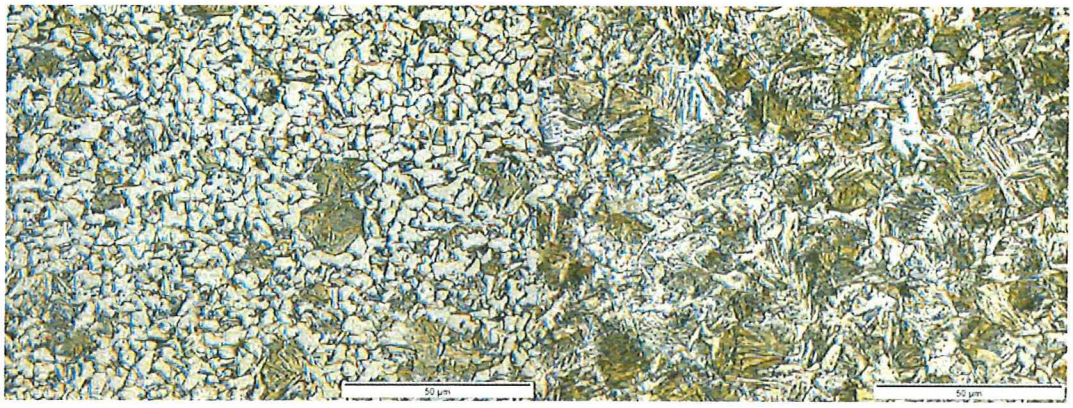

g h

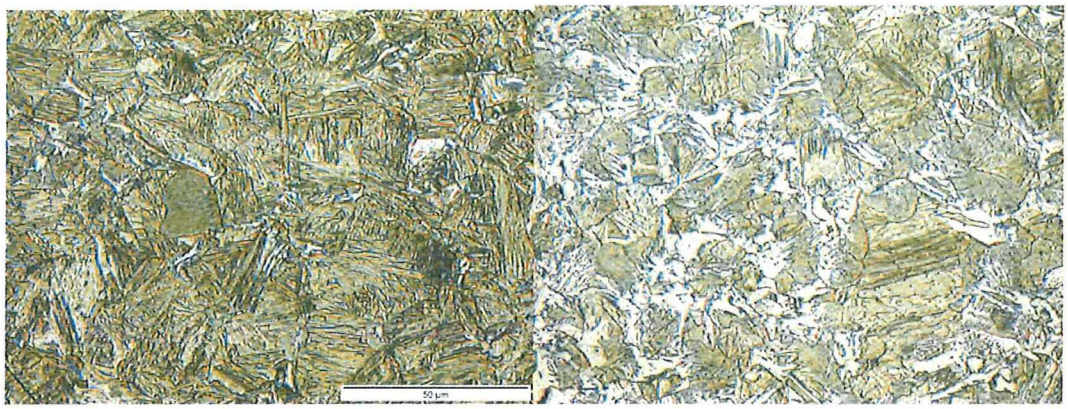

i j

Figure 37: Micrographs of samples heated and subsequently quenched. Pictures on the left hand side were heated at 400 °C/s and on the right hand side at 800 °C/s. a) and b) were heated respectively to 645 and 650 °C, c) and d) both to 695 °C, e) and f) to 770 and 800 °C, g) and h) to 870 and 865 °C and finally i) and j) both to 975 °C.

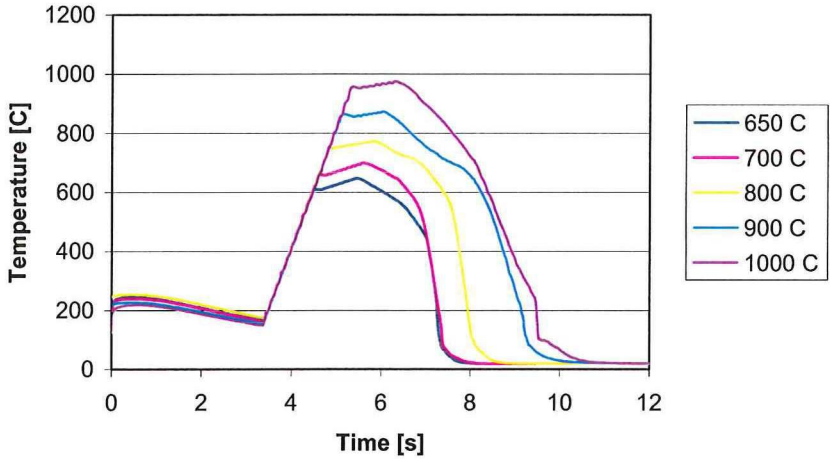

Figure 38: Temperatures during heat cycle at a heating rate of 400 °C/s

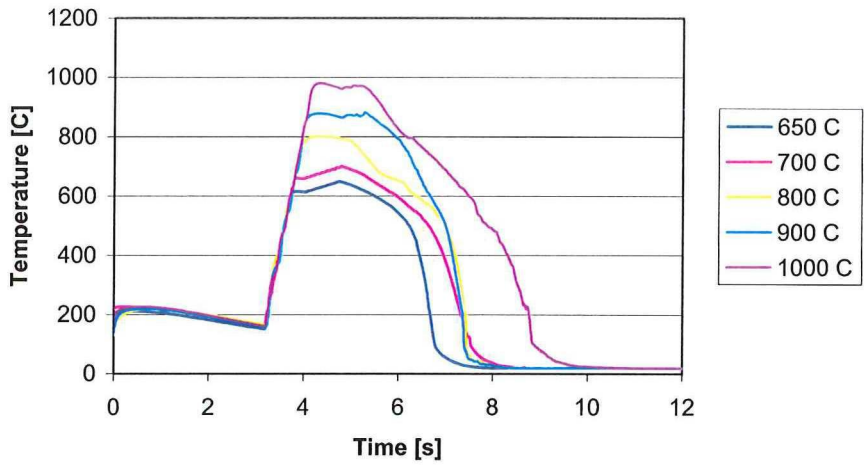

Figure 39: Temperatures during heat cycle at a heating rate of 800 °C/s

Cooling by atomised water spray did not fully transform the austenite into martensite at the applied cooling rates of up to 200 °C/s as can be concluded from the CCT diagram (Figure 8), which makes the interpretation of the results harder. Especially the samples heated to 900 °C have a very different cooling (the cooling speed of the sample that was heated at 800 °C/s was higher; see Figure 38 and Figure 39). But still it is expected that the austenite forms different transition products, enabling the possibility of making a distinction between the non transformed ferrite and transformation products.

Up to 700 °C there is hardly any difference between the samples heated at 400 and 800 °C/s, because the transition temperature is around 700 °C and no austenite forming is expected.
In the specimens that were heated at 800 °C/s the transformation occurred faster due to higher superheating. At 400 °C/s the material had the chance to temper and transform relatively slowly to austenite while some ferrite remains and can recrystallise at around 800 °C. At 800 °C/s the transition to austenite is forced, but at higher temperatures the formation of austenite at 400 °C/s is more stable and complete, which is also a result of the longer time spent at high temperatures. The cooling speed of the specimen heated to 1000 °C at a rate of 800 C°/s was slower than the one at 400 °C/s. The first was cooled from 800 °C to 500 °C in a time of 1.7 seconds (175 °C/s) and the second at 1.1 seconds (275 °C/s). The first can allow austenite to ferrite transformation while the second will only form martensitic structures according to the CCT diagram.

The transition at these rates can start as soon as 800 °C and will be complete at 1000 °C at high rates. The steps are quite large and due to the varying cooling speeds, quantitative analysis cannot be executed.

Grain refinement occurs already as a pure temperature dependent feature around 800 °C, which means that in welding the recrystallisation does not need activation by the upset movement.

4.1.2.3 Forging temperature

The temperature dependency of the stroke can be seen in Figure 40. Note that a higher rate also means a shorter time in which the material is able to deform. Stress has a clear influence on the deformation rate, while the influence of the heating rate is harder to estimate, because deformation times are shorter. Forging temperatures seem to be almost equal (700 °C) for all these circumstances.

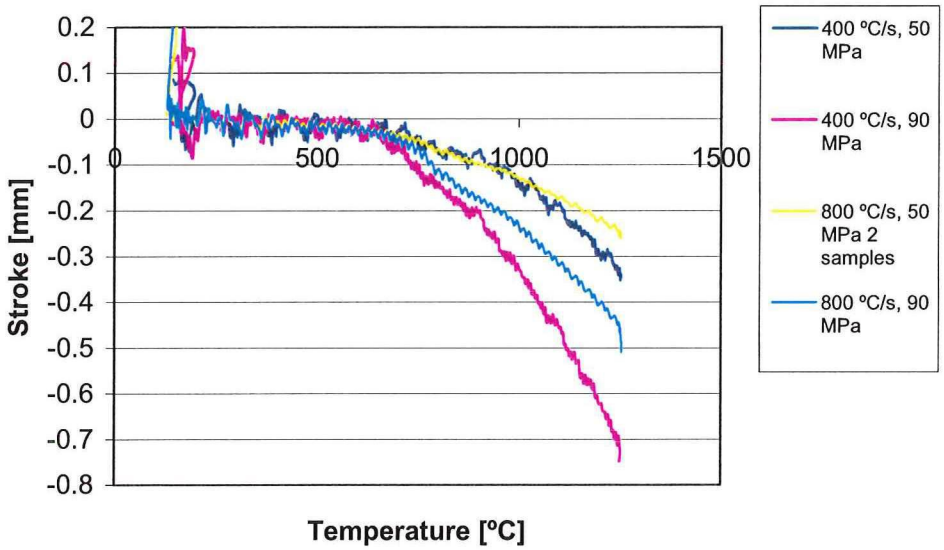

Figure 40: Stroke as a function of temperature at varying stresses and heating rates

4.2. Further discussion

The results did not yet give conclusive answer on the correct parameter setup because the fluctuations in welding parameters were too large and the existence of the hot spots gave uneven

properties along the weld. Although this seems to be a major set back, a lot understanding on the process is gained and predictions will get easier.

Since heat creation is only sufficient when current densities were at least 90 A/mm^2 and hot spot formation already occurred in this area, hot spot formation is unavoidable in the current parameter set up. The effects of these extra heated places were the melting and subsequent crack forming from the pores created. Therefore the hot spot formation can be considered as a negative feature for HR 45 sheet of 1.6 mm thickness.

Still welds with sufficient quality in the middle of the weld seam were obtained which indicates that the weld ferrite-pearlite microstructure itself is not a cause for specific failure on the weld line.

4.2.1 General on welding

Alignment and the thin plate thickness are contemporary worries on the process. A misalignment in a thinner sheet will have greater consequences during welding due to increased possibility of buckling or plates pushing past each other instead of an upset butt weld movement. In the experiments a small but constant angle (2-3°, see also Figure 4c) was found and also an asymmetrical upset formation. Even with these misalignments good welds have been obtained, but the exact influence on the process and especially the bonding should be investigated. When misalignments occur and unsatisfactory material flows can develop during welding, which leave contaminants on the interface. This in turn can be a cause for failure. The larger upset size at the lower side also originates from the misalignment, which has an angular component as showed in Figure 4c.

The rate of deformation at a low, but constant pressure level comparable to the upset butt weld pressure is not significantly increased with temperature up to 1200 °C. Temperature measurements were not executed with repeatable results, therefore it is hard to verify whether the extent of softening in the welded samples was higher. But due to the high speed deformations that have been obtained in welding experiments and simultaneously a low speed in a forging regime it is believed that the weld samples had a temperature above 1200 °C. Welds that were completely welded in a forging manner, so with no extensive softening, probably did not reach temperatures over 1200 °C. The forged welds were all considered to have insufficient bonding and therefore it is expected that softening is needed to obtain acceptable joints over the range of pressures examined. In some of the forged specimens clear remains of the interface and the contaminants have been observed, suggesting that when softening occurs, the material flows are more likely to break up the outer surface layer and disperse it along the weld zone.

At high temperatures a more effective deformation action can be obtained during deformation when the deformation rate decreases, which implies a lower upset stress with higher contact resistance. The beneficial effects of this rate decrease are limited, as at very low pressures when the contact resistance increases to a level where the rim itself will be a current path with a relative low resistance and relatively higher current, the efficiency of the process decreases.

The hot spot formation is still often regarded as a positive feature; however in opposition to the steel grades that are currently applied, HR45 is too sensitive to the high temperatures. When the hot spot appearance is prevented, welds with evenly distributed formability can be obtained. Welds with sufficient quality can be obtained, but the process must become robust and not dependent on minor interface changes. The microstructural features did not seem to cause significant alterations to the deformation characteristics of the metal.

The crack forming after intergranular melting that is associated with the hot spots can be avoided by an even heat distribution.

At low pressure the welds with the best mechanical properties were obtained, probably due to higher local heat generation, making the interface more mobile so that it can redistribute in the weld zone. Simultaneously the heat generation is more sensitive to the interface properties and the exact manner of contact. This makes the setup also less repeatable due to changes in the applied thermo-mechanical treatment.

At the moment the alignment has been improved and the first tests indicate that the forging action is significantly improved, with a bead shaped upset on both the upper and lower sides. The hot spot formation is not altered by the alignment improvement.

Hot spots

Currently it is being investigated whether the hot spot formation is due to the electromagnetic forces that act on the current or that eddy currents are involved. Turbulence can be minimised by adjusting the frequency so that the penetration depth is larger than the width of the sheet. When no significant change in the place of the hot spots occurs, eddy currents will not play an important role in their formation.

Some other explanations were found but lacked any convincing theoretical or experimental backup. These were converging of the current at the jaw-sheet interface, heat reflection at the specimen side edge, electrode bending and local increase of electron excitation at edges. Although these features might occur the extent is estimated to be small or would not *per se* cause local increase of the current density.

Microstructure

Optical microscopy cannot resolve the small features of the second phase, neither before nor after welding. After phase identification with SEM and hardness measurements, the microstructure of the base metal was classified as an allotriomorphic ferrite matrix with an average grain size of 7 μm, and upper bainite. Ferrite morphology after welding consisted of a lathlike morphology (thickness ~ 1 μm) that grew predominantly from the austenite grain boundary. Some ferrite that has a similar growth system but nucleates within the grain has been observed. This morphology is called Widmanstätten ferrite and has small particles of irresolvable second phase in between the ferrite fingers.

The large crystals of second phase were identified as non-lamellar pearlite after determining the orientation relationship with the prior austenite and hardness (200 HV_{50g}), which was too low for bainitic structures (~ 400 HV).
Mechanical tests on whole plate specimen showed a formability that was comparable to but less than the base material and therefore the microstructure is not considered to be the main reason for failure.

4.2.2 Specific experiments

Segregation

The positive attitude to expect to see the segregation profiles with optical microscopy was too optimistic. Also the segregation band in the welded specimens continued in the weld metal, so homogenisation or more severe segregation will not occur extensively. The diffusion paths for manganese will be too slow and a short period at high temperature is applied, which is far too short to cause homogenisation. The segregation band can include gaps after hot rolling, which can connect when pressure is applied

Austenitisation

For the determination of an exact amount of austenite formed, more measurements of the fraction transformed to austenite are needed. At these high heating and cooling rates, the Gleeble is acting on the edge of it's capabilities, which is mostly indicated by the discontinuous current for heating. In this fast process it can be hard to exclude small differences and guarantee a complete similar treatment. An adjustment to the experiment would be the use of a normal water spray instead of a water nebula during cooling to ensure martensitic transformation.

Forging temperature

The transition to forgeable material occurs at 700 °C for the applied heating rates and pressures. Although it seems strange that a 400 °C/s heating rate difference does not show a significant change in forging temperature, it can be that in this range of heating rates a minimum forging temperature can be determined, which might include the influence of a phase transformation. The rate of transformation will be limited by kinetics and therefore the shift in forging temperature will be minimal.

The observation that the ferrite-bainite structure does not instantaneously transform to austenite seems to contradict the origin of the forging temperature. But another feature, recrystallisation, can occur without adding strain to the base material at 800 °C as observed in the austenitisation experiments. When stressed, the deformational energy will lower the activation energy that is needed for the initiation of recrystallisation and thus recrystallisation can already start below the austenitisation temperature. It is also a diffusional controlled process and therefore can have the same kinetic limitations as discussed for a ferrite-austenite transition.

5. Conclusions and recommendations

From the experiments undertaken the following conclusions can be drawn for the weld parameters current density, upset force, distance and speed:

- A current density of 80 A/mm^2 results in insufficient heat dissipation, and the forging action cannot be executed as desired.
- At 90 A/mm^2 the required upset distance is acquired, but the upset action is partially or wholly executed in a forging regime. The material closest to the interface that is initially deformed can be softened.
- From 100 A/mm^2 and higher the material is totally softened, resulting in a smooth upset movement.

The applied force is especially influential on the heating process. A low pressure results in a high resistance, and thus more heat dissipation. It also makes the process more susceptible to variations of the interface properties and the repeatability of the process decreases. High pressures result in undesired weld shapes with a crevice in the middle of the weld. This effect is not only a result of the high pressure, but also misalignment.

The upset distance is a less important factor in the welding process than the parameters mentioned above. At three millimetres upset distance weld properties have been obtained which are comparable to those of the five millimetres upset samples, welded at the same parameter combination. Between these samples the only difference is the forging action, which means that the interface contaminants can be dispersed differently over the weld zone, but this has not been observed. The required upset distance can be obtained at lower current densities, as the amount of material that has to be heated is less than in the five millimetre samples. When the weld formability for the three and five millimetres upset samples is consistently the same, the three millimetres upset distance is preferred for the lower energy and material consumption.

A good indication for the difference between forging and softening is the upset speed. Forging has a lower (max. 15 mm/s) speed and irregular deformation pattern as result, while as the specimens are softened, the speed can reach values of up to 30 mm/s, and the deformation is executed in a smooth manner. The reason for the differences between forging and softening originates from high temperature material properties. When the material is forgeable, only

recrystallisation and recovery occur, while at higher temperatures where the material is softened, the matrix microstructure has transformed from ferrite to austenite, which has a higher rate of recrystallisation.

Local increase of the current density has been observed at both ends of the weld seam. This causes a faster heating in these places, hence the name hot spots. The effect is possibly associated with two electromagnetic effects, Lorentzforces and eddy currents, and further investigation on this subject should be undertaken. Hot spot formation causes HR 45 of 1.6 mm thickness to undergo intergranular melting. Together with the applied deformation, the material will crack locally.

Bonding is hampered by the contaminants on the interface as well as the misalignment. The contaminants remain on the bond line and are initiation points for cracks.

Misalignment causes the material to flow in an asymmetrical pattern and leaves an undesired weld shape, which is more susceptible to mechanical failure.

In determining the base and weld microstructure, optical microscopy could not give conclusive answers concerning the nature of the phases formed. SEM analysis reveals most microstructural features, but not to a degree where the difference between the displacive growth of bainitic ferrite and the diffusional growth of pearlitic ferrite could be observed. For this purpose TEM analysis should be undertaken.

The weld microstructures obtained between the hot spots consisted of Widmanstätten ferrite and non-lamellar pearlite, which have formability properties comparable to the base material.

The forging temperatures for heating rates of 400 and 800 °C/s were both 700 °C, indicating that although the superheating might be larger at 800 °C/s, the kinetics of recrystallisation or recovery were a limiting factor in the softening of the material.

The transformation to austenite at rates of 400 and 800 °C/s was completed at 1000 °C, but the precise fraction as a function of time and temperature could not be determined, as the cooling rates did not always give a martensitic transformation. In the transition area the number of measurements also was too small to extract conclusive data on the transformation speed.

Since the misalignment was a factor that influenced the weld process to a significant extent, the influence of the segregation band that crosses the surface on crack initiation could not be studied. Whether the segregation is extended or the constituents homogenise during the heat treatment during welding has not been established. More analysis with equipment that can measure composition (like SEM or X-ray diffraction) is needed to be able to describe the influence of heat

treatment on segregation. In the weld experiments, segregation was observed within the weld zone, indicating that the thermo-mechanical treatment of welding does not homogenise the band.

From the combined results of this study it is considered that for the HR 45 material, the origin of the poor formability lies within the weld set-up and not the microstructure obtained. Especially the misalignment and the hot spot formation hamper the formation of a good uniform bond line. The misalignment can and is already altered and weld shape has become more symmetric. Alterations to the current application might decrease the hot spot formation, but to what extent this is obtainable with the current power source should be further investigated. It is expected that when these negative influences are minimised a weld sequence that gives welds with good bonding is obtainable. The experiments undertaken were performed with milled interfaces; the role of the more irregular sheared interfaces is neglected and should be incorporated in further research.

Recommendations

To be able to describe the process properly, temperature measurement should be undertaken. This is a determining parameter for the forging conditions and the final weld properties. For the short weld process a high speed measuring method, like thin thermocouples or a high-speed infrared camera is required.

A better distinction can be made between forging and softening conditions in terms of temperature and pressure intervals. Theoretically this transition should be a result of austenitisation, and the measurements on the phase transformation might give insight into this feature. Also, these intervals themselves can be determined more precise.

After the latest improvement of the alignment a better repeatability at low pressures is expected, but hot spot formation is not eliminated.

To prevent hot spot formation, the frequency of the current application should be included as a variable parameter. A change in frequency is desired to alter the turbulence so that the hot spot formation is less extensive.

After a decrease of the hot spot formation and the change of alignment, the welding experiments should be repeated to optimise the weld parameter combination. After stabilisation of the process this might have shifted and become more robust, enlarging the parameter window.

To obtain a full metallurgical overview on the process more precise experiments should be undertaken on the austenitisation, recrystallisation and the cooling transformations. Austenitisation and recrystallisation control the smoothness of the upset movement as well as the austenite grain size, and therefore the final microstructure. The transformation upon cooling determines the morphology of the ferrite and second phase and with these microstructural features, the weld formability can be optimised.

Acknowledgements

The author would like to thank his committee of this project: Prof. Dr. Ian Richardson for the supervision, Ir. Niels Kerstens for his supervision and continuing daily support, Ir. Rudolf Meulenberg from Fontijne Grotnes, Prof. Dr. Jilt Sietsma and Dr. Marcel Hermans. Especially Rudolf Meulenberg and Gerrit Nauss at Fontijne Grotness are gratefully acknowledged for providing the welding equipment. The next persons are acknowledged for the discussions and ideas on the microstructure, Dr. Iman Maroef, Erik Peekstok and Dr. Stefan van Bohemen. The Joining and Mechanical Behaviour group (especially room 182) as well as the people of the material science student society "Het gezelschap Tubalkaïn" at Delft University of Technology are thanked for their listening capabilities and support during the project.
Sullivan Smith at Corus is acknowledged for providing the Erichsen deformability test apparatus. For the selfless reading and comments during the writing of this thesis Herr Doctor Kees Bos and Ir. Jan Jongerden are acknowledged. Finally the author would like to thank his parents, his sister and Astrid Broeders for their support, even though they had not the faintest idea what the author was prattling on about.

Literature

1. Jol, B.J.A., *Upset butt welding of ferrite bainite high resistance steels.* 2005, Netherlands Institute for Metal Research: Delft. p. 38.
2. Kanne Jr., W.R., *Upset welding*, in *ASM handbook: welding brazing and soldering*, D.L. Olson, et al., Editors. 1993, The materials Information society. p. 249-251.
3. Naus, G.J.L., *DC upset resistance welding; Modelling and control of a weld process*, in *Department of Mechanical Engineering*. 2005, University of Technology Eindhoven: Eindhoven. p. 98.
4. Ghosh, P.K., et al., *Studies on microstructure and HAZ hardness of flash butt welded Mn-Cr-Mo dual phase steel produced under different weld thermal cycles.* Transactions of the Indian institute of metals, 1992. **45**(6): p. 399-408.
5. Krishnaraj, N., K. Prasad Rao, and E.G. Ramachandran, *The Quality of Flash Welded Joints in Mild Steel: A Study on the effects of Welding Parameters.* Welding Journal, 1993. **72**(6): p. s239-s245.
6. Kleiber, M. and A.S. Sluzalec jr., *Numerical analysis of heat flow in flash welding.* Archives of Mechanics, 1983. **35**(5-6): p. 687-699.
7. Wray, P.J., *Mechanical, physical and thermal data for modeling the solidification processing of steels*, in *Modeling of Casting and Welding Processes*, H.D. Brody and D. Apelian, Editors. 1981, The metallurgical Society of AIME: Warrandale.
8. Kobayashi, A., et al., *Study on the Amount of Upset of Friction Welding (Experimental Equation on the Amount of Upset of Same Kind SC Steel).* JSME International Journal, 1989. **32**: p. 385-390.
9. Dong, S.J., G.P. Kelkar, and Y. Zhou, *Electrode sticking during micro-resistance welding of thin metal sheets.* Ieee Transactions on Electronics Packaging Manufacturing, 2002. **25**(4): p. 355-361.
10. Holm, R., *Electrical Contacts, Theory and Applications.* 1967: Berlin, New York.
11. Zwolsman, J.O. and H.M. Vroomans, *Der Contactwiderstand beim Widerstandschweissen.* DVS berichte, 1987. **124**: p. 122-127.
12. Kerstens, N.F.H., *Investigation and control of factors influencing resistance upset welding.* 2005, Delft, University of Technology: Delft. p. 87.
13. Udin, H., *Welding for engineers.* 1954: John Wiley and sons.
14. den Ouden, G., *Lastechnologie.* 1993, Delft: Delftse Uitgevers Maatschappij b.v. 203.
15. Walton, A.J., *Three phases of matter.* 2nd ed. 1983, Oxford: Oxford University Press. 482.
16. Smith, S., *Concentrated current due to electrode bending?*, B.J.A. Jol, Editor. 2005: IJmuiden.
17. JEOL, *A Guide to Scanning Microscope Observation.* 2003. p. 36.
18. Ohring, M., *The Materials Science of Thin Films.* 1st ed. 1992, New Jersey: Academic Press. 704.
19. Vaidyanath, L., M. Nicholas, and D. Milner, *Pressure welding by rolling.* British Welding Journal, 1959. **6**: p. 13-28.
20. Nied, H.A. *Interface displacement characteristics of upset welding.* in *Recent trends in Welding Science and Technology.* 1989. Gatlinburg, Tennessee: ASM International.
21. Souami, N., et al., *Carbon segregation and Inclusions Effects on Surface Fracture Morphology of 1 12% Chromium Stainless Steel.* Journal of Materials Engineering and Performance, 2003. **12**(6): p. 715-720.

22. Poirier, D.R. and G.H. Geiger, *Transport Phenomena in Materials Processing*. 1994, Warrendale, Pennsylvania: The Minerals, Metals and Materials Society. 658.
23. Cacciatore, P., *Modeling of heat transfer in welding processes*, in *Modeling of Casting and Welding Processes*, H.D. Brody and D. Apelian, Editors. 1981, The Metallurgical Society of AIME: Warrendale. p. 113-126.
24. Debray, B., P. Teracher, and J.J. Jonas, *Simulation of the Hot Rolling and Accelerated Cooling of a C-Mn Ferrite Bainite Strip Steel.* Mettallurgical and Materials Transactions A, 1995. **26A**(1): p. 99-111.
25. Katsumata, M., et al., *Relationship between microstructure and mechanical properties in direct quenched low carbon HSLA steels used in as-hot forged conditions*, in *Physical Metallurgy of Direct -Quenched Steels*, K.A. Taylor, S.W. Thompson, and F.B. Fletcher, Editors. 1993, The Minerals, Metals & Materials Society. p. 247-263.
26. Teracher, P. and G. Marron, *Application of high-strength, hot rolled steels in wheels.* JOM-JOURNAL OF THE MINERALS METALS & MATERIALS SOCIETY, 1996. **48**(7).
27. Bhadeshia, H.K.D.H., *Bainite in steels*. 2nd ed. 2001, Cambridge: IOM Communications Ltd. 454.
28. Bhadeshia, H.K.D.H. and J.W. Christian, *Bainite in Steels.* Metallurgical Transactions A, 1990. **21A**: p. 767-797.
29. Nieuwstraten, M., *Chemisch onderzoek*. 2005, Schielab b.v.: Rotterdam. p. 1.
30. Aliya, D. and S. Lampman, *Physical Metallurgy Concepts in Interpretation of Microstructures*, in *Metallography and Microstructures, Vol 9, ASM Handbook*. 2004, ASM international.
31. Sakaki, T., K. Sugimoto, and T. Fukuzato, *Role of Internal-Stress for Continuous Yielding of Dual-Phase Steels.* Acta Metallurgica, 1983. **31**(10): p. 1737-1746.
32. Speich, G.R., *Dual-Phase Steels*, in *ASM Handbook vol 1, Properties and selection: Irons, Steels, and High-Performance Alloys*. 1990. p. 424-429.
33. Humphreys, F.J. and M. Hatherly, *Recrystallization and Related Annealing Phenomena.* 1st ed. 1996: Elsevier Science Ltd. 497.
34. Smith, A., *Simulation of Recrystallisation*. 2002, Delft University of Technoloy: Delft. p. 50.
35. Porter, D.A. and K.E. Easterling, *Phase Transformations in Metals and Alloys*. 2nd ed. 1992: Chapman & Hall. 514.
36. McQueen, H.J. and C.A.C. Imbert, *Dynamic recrystallisation: plasticity enhancing structural developement.* Journal of Alloys and Compounds, 2003. **378**: p. 35-43.
37. Kwon, O. and A.J. DeARDO, *On the recovery and recrystallization which attend static softening in hot-deformed copper and aluminum.* Acta metallurgica et materialia, 1990. **38**(1): p. 41-54.
38. Metals, T.d.s.M.C.i., *viewCCT*. 2001, Delft University of Technology: Delft.
39. Todorov, R.P. and K.G. Khristov, *Widmanstatten structure of carbon steels.* Metal Science and Heat Treatment, 2004. **46**(1-2): p. 49-53.
40. Nagasaki, C. and J. Kihara, *Evaluation of intergranular embrittlement of a low carbon steel in austenite temperature range.* Isij International, 1999. **39**(1): p. 75-83.
41. Jol, B.J.A., *The reaction of segregation bands in high resistance steels on thermomechanical treatment*, N.F.H. Kerstens, Editor. 2004: Delft.
42. Grube, W.L. and S. Verhoff, *Plasma (Ion) Carburizing of Steels; General Process Characteristics*, in *ASM handbook, Volume 4, Heat treating*. 2002, ASM.
43. Fujita, M., *Diffusion Database of various Elements in Iron-Base Solid Solution*. 1996.
44. Nohara, K. and K. Hirano, *Self-Diffusion of Fe in Fe-Mn Alloys.* Izv. Vyssh. Ucheb. Zaved., Chem. Metall, 1977: p. 110-113.
45. *Testing methods*, steel-n.com.

46. NEN, *ISO 9015-2:2003: Destructive tests on welds in metallic materials - Hardness testing - Part 2: Microhardness testing of welded joints*, in *Destructieve beproevingen van lasverbinding in metalen - Hardheidsmeting - Deel 2: Microhardheidsmeting van gelaste verbindingen*. 2003. p. 9.
47. ASM, *BS EN 1043-2:1997*
Destructive tests on welds in metallic materials. Hardness testing. Micro hardness testing on welded joints. 1997. p. 14.
48. SAE, *ASTM E 92: STANDARD TEST METHOD FOR VICKERS HARDNESS OF METALLIC MATERIALS*. 2004. p. 9.
49. Sharma, P., P.K. Ghosh, and S.K. Nath, *Fatigue Behaviour of Resistance Spotwelded Mn-Cr_Mo Dual Phase Steel*. Zeitschrift fur Metallkunde, 1993. **84**(7): p. 513-517.
50. Modin, H. and S. Modin, *Metallurgical Microscopy*. 1973, Stockholm: Meritforlaget. 473.
51. Kilpatrick, J.R., A.O. Benscoter, and A.R. Marder, *Tint Etching Improves Resolution and Contrast of Microstructures*. Metal Progress, 1971. **100**(6): p. 79-81.
52. Voort, V., *Tint etching*. Metal Progress, 1985: p. 31-41.
53. Debray, B., M. Babbit, and J.J. Jonas, *Structure and properties of an as-hot rolled ferrite bainite plain carbon steel*, in *Physical Metallurgy of Direct-Quenched Steels*, K.A. Taylor, S.W. Thompson, and F.B. Fletcher, Editors. 1993, The Minerals, Metals & Materials Society. p. 155-168.
54. LePera, F.S., *Improved Etching Technique for the Determination of Percent Martensite in High-Strength Dual-Phase Steels*. Metallography, 1979. **12**: p. 263-268.
55. Beraha, E. and B. Shpigler, *Color Metallography*. 1 ed. 1977: American Society for Metals. 160.
56. Casimir, H.B.G. and J. Ubbink, *Het skineffect*. Philips technisch tijdschrift, 1967. **28**(6): p. 173-185.
57. Mett, R.R., et al., *Electron paramagnetic resonance field-modulation eddy-current analysis of silver-plated graphite resonators*. Review of Scientific Instruments, 2005. **76**(9): p. -.
58. Bramfitt, B.L. and J.G. Speer, *A Perspective on the Morphology of Bainite*. Metallurgical Transactions a-Physical Metallurgy and Materials Science, 1990. **21**(4): p. 817-829.
59. Ohmori, Y., *Microstructural evolutions with precipitation of carbides in steels*. Isij International, 2001. **41**(6): p. 554-565.
60. Thewlis, G., *Classification and quantification of microstructures in steels*. Materials Science and Technology, 2004. **20**(2): p. 143-160.
61. Samuels, L.E., *Transformation of Austenite*, in *Light Microscopy of Carbon Steels*. 1999, ASM. p. 500.
62. Savran, V.I., *Determination of a lath/plate like morphology in HR45*, B.J.A. Jol, Editor. 2005: Delft.
63. Stewart, J.W., J.A. Charles, and E.R. Wallach, *Iron-phosphorus-carbon system Part 3 - Metallography of low carbon iron-phosphorus alloys*. Materials Science and Technology, 2000. **16**(3): p. 291-303.